Integrated Structural Analysis and Design

using 3-D Finite Elements

by

Uma Madapur

Thesis submitted to the Faculty of the

Virginia Polytechnic Institute and State University

in partial fulfillment of the requirements for the degree of

Master of Science

in

Aerospace & Ocean Engineering

APPROVED:

R Haftka

R.T. Haftka, Chairman

Rakesh K. Kapania

R.K. Kapania

Z. Gurdal

Z. Gurdal

May 1988

Blacksburg, Virginia

LD
3855
V855
1988
M323
c. 2

Integrated Structural Analysis and Design

using 3-D Finite Elements

by

Uma Madapur

R.T. Haftka, Chairman

Aerospace & Ocean Engineering

(ABSTRACT)

When structural analysis is performed via iterative solution technique it is possible to integrate the analysis and design iterations in an integrated analysis and design procedure. The present work seeks to apply an integrated analysis and design approach due to Rizk to the problem of hole shape optimization in thick plates.

The plates are modeled by three dimensional eight noded elements. An element by element (EBE) preconditioned conjugate gradient (PCG) method is used for the structural analysis, because this method is well suited for poorly banded three dimensional problems. The plates were optimized so as to minimize the stress concentration near the hole measured by the ratio of the Von Mises stress to the applied boundary stress. The analysis program was validated by comparision to a commercial finite-element program as well as photoelastically obtained stress concentrations. Similarly, the optimization procedure was checked against plates optimized by a photoelastic technique. Good agreement was observed.

The integrated analysis and design approach tested here is based on partially converged solutions of the EBE-PCG iterative process. A study of the effect of the number of iterations on analysis and derivative accuracy was performed. Based on this analysis a

choice was made for the number of iterations to be used in the integrated analysis and design procedure. It was found that the cost of the design could be significantly reduced with only minimal effects on the final shape and stress concentration factor.

Acknowledgments

I am indebted to Dr. R.T. Haftka for the help and guidance he has given me throughout this work. I wish to thank Dr. R.K. Kapania and Dr. Z. Gurdal for serving on my committee.

I take this opportunity to thank all my friends for their help and advice, and my husband for the constant encouragement.

This thesis is dedicated to my loving parents.

TABLE OF CONTENTS

LIST OF TABLES

LIST OF FIGURES

NOMENCLATURE

$\mathbf{B}$	Preconditioner Matrix
$\mathbf{D}^e$	Diagonal of Element Stiffness Matrix
$\mathbf{f}$	Force Vector
$\mathbf{K}$	Stiffness Matrix
$\mathbf{K}^e$	Element Stiffness Matrix
N	Number of Iterations for EBE-PCG
nele	Number of Elements
nnb	Number of Nodes on the Boundary
nr	Number of terms in the Radius series
r	Residue in CG
ρ	Spectral Distance of a Matrix
σ_{von}	Von Mises Stress
$\mathbf{u}$	Displacement Vector
$\mathbf{W}$	Scaling Matrix
ω	Relaxation Parameter
$\mathbf{X}$	Design Parameters

Chapter 1. Introduction

Structural optimization was initially based on the calculus of variations. A typical problem was solved by obtaining the Euler-Lagrange optimality differential equations and solving them simultaneously with the differential equations of the structural response. This approach is still used for the optimization of individual structural elements, however for built-up structures modeled by finite elements, a nested approach is typical. The structural response is calculated for a given set of design variables. The derivatives of the response with respect to design parameters are used in directing the optimization search and updating the design parameters. This two phase approach is called the nested (or inner outer) approach Fig. 1.

In the last twenty-five years direct search methods have been gaining ground as the standard for structural optimization. These techniques are commonly used in a nested approach. That is, the structural analysis equations are repeatedly solved during each design iteration. Part of the reason for the popularity of the nested approach is that the structural analysis equations are solved by techniques which are quite different from those used for the design optimization. An exception is the design of a structure subject

to constraints on its collapse load. There, the analysis problem ("limit analysis") is often approximated as a linear program and solved by the simplex method. The structural design problem in that case ("limit design") is easily formulated as a single linear program with the element forces and structural parameters both treated as design variables [1].

In the late sixties, Fox and Schmit [2] and their coworkers (Schmit, Bogner and Fox [3], Fox and Stanton [4], Fox and Kapoor [5]) tried to integrate structural analysis and design by employing conjugate gradient (CG) minimization techniques for solving linear structural analysis problems. They found that the optimization methods were not competitive with the traditional direct Gaussian elimination techniques. More recently, techniques for unconstrained minimization have improved to the point where they can be competitive with elimination techniques for poorly banded problems [6].

The simultaneous analysis and design approach replaces the outer level of constrained optimization and the inner level of structural response solution by a single constrained optimization problem. The structural response (equilibrium) equations are treated as equality constraints, and the structural response variables are additional variables in the optimization problem. The approach benefits from the developments in unconstrained optimization for structural analysis [6] and use of element by element (EBE) approach to preconditioned conjugate gradient (PCG) method for structural analysis [7, 8]. Such an approach demonstrated substantial computational savings over the nested approach for both the linear and non-linear truss optimization problems [9, 10]. However the convergence and computational cost are quite sensitive to the conditioning of the stiffness matrix.

A different technique for integrating the analysis and design is the single cycle approach proposed by Rizk [11] for aerodynamic design, when the analysis problem is solved by an iterative approach. The single cycle approach updates the design parameters after every analysis iteration or every *Nth* iteration where *N* is considerably less than the total number of iterations required for full convergence in the analysis. The name derives itself from the practice of updating both the structural response and the design variables in the same cycle. The design variables are based on an approximate response. Both response and design converge simultaneously to their solutions. The method could be applicable to structures which can be analyzed more efficiently by iterative schemes like the conjugate gradient method than by direct methods like Gaussian elimination. Rizk approach was applied to structural optimization under constraint on nonlinear behaviour by Haftka [12]. In that application the nonlinear load iteration was integrated with the optimization iteration.

The simultaneous analysis and design merges the analysis level and the optimization level, while the integrated analysis and design still maintains the two levels as in nested approach, but the inner level goes only to partial convergence. The dimensionality of the problem increases in the simultaneous analysis and design approach because the response variables are also considered as design variables and this increased dimensionality can increase computational cost and storage requirements. The purpose of the present work is to test the application of Rizk's approach to structural design in the linear range. Another objective is to employ 3-dimensional finite elements which often benefit from an iterative solution approach because they result in poorly banded equations.

Rizk's single cycle (Integrated analysis and design) approach is applied to finding the optimum shape of a central hole in a thick plate under uniaxial loading, so as to minimize the stress concentration in the plate. The plate is modelled by three dimensional eight noded brick elements. The displacements are found using EBE PCG scheme.

Shape optimization problems have received much attention in recent years. In terms of a finite element model we consider as shape variables any design variables which have control over the location of the nodes. Early work in structural optimization was concerned mostly with truss structures. This followed the work of Michell [13] who developed the theory of optimum truss layout when there is no limit on the number of joints. The theory of Michell trusses is still being pursued [14, 15] and have also been extended to grillages [16]. While problems of geometry and topology in truss design occupied researchers in early and mid-seventies, recently there has been a veritable explosion of interest in shape optimization of plate, shell and solid components [17-20]. The method used for these shape optimization problems range from calculus of variations [21] to experimental optimization employing photoelastic models [18, 19]. However most of the work is based on employing mathematical programming methods coupled with finite element analysis of the structure. The major problem in the shape optimization of a structure modeled by two or three dimensional finite elements is the deformation of the mesh. There is the danger of obtaining meshes with excessively deformed finite elements. Hole shape optimization problems have been dealt with extensively in the literature for thin plates. Experimental optimization using photoelastic techniques results have been presented by Durelli et. al. [18, 19]. Dhir presented analytical solutions for optimizing the geometry of a class of hole shapes for large plates [20].

Chapter 2 gives an overview of the EBE PCG scheme. Chapter 3 describes the problem and the single cycle approach for the problem. Chapter 4 include results and discussion for the approach.

Chapter 2. Iterative Solution of Static Response

2.1 Equation of Static Response

The equations of equilibrium of a structure obtained by a finite element formulation are typically written as

$$\mathbf{Ku} = \mathbf{f} \tag{2.1.1}$$

where **K** is the stiffness matrix obtained by assembly of element matrices, **u** is the displacement vector, and **f** is the force vector.

K is a *nxn* symmetric, positive definite matrix where n is the number of structural degrees of freedom. Equation 2.1.1 can be solved directly or indirectly by iterative methods.

2.2 Solution of Linear Equations

Non-iterative solution methods include elimination and factorization methods such as Gauss and Gauss-Jordan elimination. One of their disadvantages is that, if the coefficient matrix is sparse , the sparsity is not fully exploited, because zeros in the matrix do not remain zeros as elimination proceeds. Inversion is also a non-iterative method, but as the calculation of $\mathbf{K}^{-1}$ is more expensive in terms of computer time than factorization, and the matrix $\mathbf{K}^{-1}$ is typically fully populated so that storage requirements are very large, it is not commonly used for large systems of equations.

Iterative methods generate a sequence of approximate solutions $\mathbf{u}^k$ where k is the iteration count, and involve the matrix $\mathbf{K}$ only multiplicatively . The evaluation of an iterative method invariably focuses on how quickly the iterates $\mathbf{u}^k$ converge to the solution. When the coefficient matrix $\mathbf{K}$ is sparse indirect methods may be preferred over direct methods because of much lower memory requirements. However the rate of convergence and hence the number of iterations may not be known in advance. In the present work we are interested in iterative method for their potential of being integrated into the design iteration. Several iterative methods are discussed below.

2.3 Jacobi and Gauss Seidel Method

Equation 2.1.1 can be rewritten as

$$u_i = (f_i - \sum_{j=1}^{i-1} K_{ij}u_j - \sum_{j=i+1}^{n} K_{ij}u_j)/ K_{ii} \qquad (2.3.1)$$

where u_i is the i^{th} component of the vector $\mathbf{u}$

The Jacobi iteration is given as [22]

$$u_i^{k+1} = (f_i - \sum_{j=1}^{i-1} K_{ij}\, u_j^k - \sum_{j=i+1}^{n} K_{ij}\, u_j^k)/\, K_{ii} \tag{2.3.2}$$

In matrix notation, equation 2.3.2.can be written as

$$\mathbf{D}_s\, \mathbf{u}^{k+1} = \mathbf{f} - (\, \mathbf{L}_s + \mathbf{U}_s)\, \mathbf{u}^k \tag{2.3.3}$$

where

$$\mathbf{K} = \mathbf{L}_s + \mathbf{D}_s + \mathbf{U}_s \tag{2.3.4}$$

and $\mathbf{L}_s$, $\mathbf{D}_s$ and $\mathbf{U}_s$ are the matrices with lower triangle, diagonal and the upper triangle of the matrix $\mathbf{K}$. If we rewrite the above approximation scheme using the most recent values of $\mathbf{u}$, then we get the Gauss-Seidel iteration scheme.

$$u_i^{k+1} = (f_i - \sum_{j=1}^{i-1} K_{ij}\, u_j^{k+1} - \sum_{j=i+1}^{n} K_{ij}\, u_j^k)/\, K_{ii} \tag{2.3.5}$$

This can be written in matrix form as

$$\mathbf{D}_s\, \mathbf{u}^{k+1} = \mathbf{f} - \mathbf{L}_s\, \mathbf{u}^{k+1} - \mathbf{U}_s\, \mathbf{u}^k \tag{2.3.6}$$

or

$$(\mathbf{D}_s + \mathbf{L}_s) \mathbf{u}^{k+1} = \mathbf{f} - \mathbf{U}_s \mathbf{u}^k \tag{2.3.7}$$

The above set of equations can be rewritten as

$$\mathbf{M} \mathbf{u}^{k+1} = \mathbf{f} + \mathbf{N} \mathbf{u}^k \tag{2.3.8}$$

where

$$\mathbf{M} - \mathbf{N} = \mathbf{K} \tag{2.3.9}$$

It can be shown [23] that if $\rho(\mathbf{M}^{-1} \mathbf{N}) < 1$ where ρ is the spectral distance of the matrix, then in the limit , $\mathbf{u}$ converges to $\mathbf{K}^{-1} \mathbf{f}$. The spectral distance of a matrix is the magnitude of its largest eigenvalue of the matrix. The rate of convergence increases as the value of ρ decreases. The condition $\rho(\mathbf{M}^{-1} \mathbf{N}) < 1$ is guaranteed by diagonal dominance of $\mathbf{K}$ for Jacobi and Gauss-Seidel iterations.

2.4 Successive Over Relaxation

An improvement on the Gauss-Seidel method for matrices when $\rho(\mathbf{M}^{-1} \mathbf{N})$ is close to 1 is given by the Successive Over Relaxation (SOR) scheme where

$$\mathbf{M}_\omega \mathbf{u}^{k+1} = \mathbf{N}_\omega \mathbf{u}^k + \omega \mathbf{f} \tag{2.4.1}$$

where

$$\mathbf{M}_\omega = \mathbf{D}_s + \omega \mathbf{L}_s \tag{2.4.2}$$

$$\mathbf{N}_\omega = (1-\omega)\,\mathbf{D}_s - \omega\,\mathbf{U}_s \tag{2.4.3}$$

and ω is a relaxation parameter.

The SOR method is the same as Gauss-Seidel if $\omega = 1$. For a few problems the value of ω that minimizes the spectral distance is known and can be used. For others, ω has to be determined by complex eigenvalue analysis.

2.5 Conjugate Gradient Method

All gradient search methods solve $\mathbf{K}\,\mathbf{u} = \mathbf{f}$ by minimizing a function $\phi(\mathbf{u})$ such that the value of $\mathbf{u}$ at which $\phi(\mathbf{u})$ is minimum is given by $\mathbf{K}^{-1}\,\mathbf{f}$. When $\mathbf{K}$ is positive definite one such function is given by

$$\phi(\mathbf{u}) = \frac{1}{2}\,\mathbf{u}^T\,\mathbf{K}\,\mathbf{u} - \mathbf{u}^T\,\mathbf{f} \tag{2.5.1}$$

The method of Steepest Descent updates the $\mathbf{u}^k$ by choosing a direction such that the function ϕ decreases most rapidly at each step. This is the direction of the negative gradient

$$-\nabla\phi(\mathbf{u}^k) = \mathbf{f} - \mathbf{K}\,\mathbf{u}^k = \mathbf{r}^k \tag{2.5.2}$$

The updating step hence is given by

$$\mathbf{u}^{k+1} = \mathbf{u}^k + \alpha^{k+1}\, \mathbf{r}^k \tag{2.5.3}$$

α is chosen so as to minimize $\phi(\mathbf{u}^k + \alpha^{k+1}\, \mathbf{r}^k)$ and is given by

$$\alpha^k = \frac{(\mathbf{r}^{k-1})^T\, \mathbf{r}^{k-1}}{(\mathbf{r}^{k-1})^T\, \mathbf{K}\, \mathbf{r}^{k-1}} \tag{2.5.4}$$

The convergence of this method may be slow. Conjugate Gradient (CG) methods instead successively minimize ϕ along a set of directions $\mathbf{p}^1, \mathbf{p}^2, \ldots$ that do not necessarily correspond to $\mathbf{r}^0, \mathbf{r}^1, \ldots$.

Hence

$$\mathbf{u}^{k+1} = \mathbf{u}^k + \alpha^{k+1}\, \mathbf{p}^{k+1} \tag{2.5.5}$$

It can be shown that [23] we can choose $\mathbf{p}^k$ such that in using the vector $\mathbf{p}^{k+1}$ to solve the one dimensional minimization problem

$$\text{min. } \phi(\mathbf{u}^k + \alpha^{k+1}\, \mathbf{p}^{k+1}) \tag{2.5.6}$$

We also solve the $(k+1)$ dimensional minimization problem which is given by

$$\text{min. } \phi(\mathbf{u}^0 + \sum_{i=1}^{k+1} \alpha^i \mathbf{p}^i) \tag{2.5.7}$$

Choosing the vector $\mathbf{p}^{k+1}$ to be K - conjugate to the vectors $\mathbf{p}^1, \mathbf{p}^2, \ldots, \mathbf{p}^k$ ensures the desired result. Such a vector has the property $(\mathbf{p}^{k+1})^T \mathbf{K}\, \mathbf{p}^j = 0,\ j = 1, \ldots, k$. Since there are many such choices for $\mathbf{p}^k$ one choice will be to choose $\mathbf{p}^{k+1}$ to be closest vector to $\mathbf{r}^k$ of all possible $\mathbf{p}^{k+1}$. Such a choice of $\mathbf{p}^{k+1}$ leads to the residuals $\mathbf{r}^k$ being mutually orthogonal. It can be further shown that $\mathbf{p}^{k+1}$ can be represented as a linear combination of $\mathbf{p}^k$ and the residual $\mathbf{r}^k$. That leads to the formulation

$$\mathbf{p}^{k+1} = \mathbf{r}^k + \beta^{k+1} \mathbf{p}^k \tag{2.5.8}$$

where

$$\beta^{k+1} = -\frac{(\mathbf{p}^k)^T \mathbf{K}(\mathbf{r}^k)}{(\mathbf{p}^k)^T \mathbf{K}(\mathbf{p}^k)} \tag{2.5.9}$$

The value of α^{k+1} can be found as explained earlier by minimizing the function ϕ , and we get

$$\alpha^{k+1} = \frac{(\mathbf{r}^k)^T(\mathbf{r}^k)}{(\mathbf{p}^{k+1})^T \mathbf{K}(\mathbf{p}^{k+1})} \tag{2.5.10}$$

This form of conjugate gradient algorithm was presented originally by Hestenes and Steifel [24].

2.6 Preconditioning

In structural problems as the stiffness matrix usually have a very high condition number the convergence of an iterative scheme can be improved by preconditioning **K** . The system of equations $\mathbf{K}\,\mathbf{u} = \mathbf{f}$ is transformed into

$$\mathbf{B}^{-1}\,\mathbf{K}\,\mathbf{u} = \mathbf{B}^{-1}\,\mathbf{f} \tag{2.6.1}$$

where **B** is the postive definite symmetric preconditioner. The CG residue which was

$$\mathbf{r} = \mathbf{K}\,\mathbf{u} - \mathbf{f} \tag{2.6.2}$$

becomes

$$\mathbf{B}^{-1}\,\mathbf{r} = \mathbf{B}^{-1}(\mathbf{K}\,\mathbf{u} - \mathbf{f}) \tag{2.6.3}$$

It is desirable that the condition number of $\mathbf{B}^{-1}\,\mathbf{K}$ be small. The smaller the condition number better is the convergence. The ideal case is $\mathbf{B}^{-1}\,\mathbf{K} = \mathbf{I}$ where the condition number is 1. However we want **B** to be easy to invert or factorize. For the PCG to be an effective sparse matrix technique the choice of the preconditioner **B** should be such

that the system $\mathbf{Bz} = \mathbf{r}$ can be solved easily, implying $\mathbf{B}$ can be easily inverted. An appropriate preconditioner $\mathbf{B}$ is needed for the practical usage of the Preconditioned Conjugate Gradient algorithm.

The algorithm for the Preconditioned Conjugate Gradient Method is given below

Step 1. Initialization

$$k = 0$$

$$\mathbf{u}^0 = 0$$

$$\mathbf{r}^0 = \mathbf{f}$$

$$\mathbf{p}^0 = \mathbf{z}^0 = \mathbf{B}^{-1}\mathbf{r}^0$$

Step 2. Update solution and residual

$$\alpha^k = \frac{(\mathbf{r}^k)^T \mathbf{z}^k}{(\mathbf{p}^k)^T \mathbf{K}\, \mathbf{p}^k}$$

$$\mathbf{u}^{k+1} = \mathbf{u}^k + \alpha^k \mathbf{p}^k$$

$$\mathbf{r}^{k+1} = \mathbf{r}^k - \alpha^k \mathbf{K}\mathbf{p}^k$$

Step 3. Convergence check

$$|| \mathbf{r}^{k+1} || < \delta$$

(δ = convergence criteria)

Yes- Return

No - Continue

Step 4. Update conjugate direction

$$\mathbf{z}^{k+1} = \mathbf{B}^{-1}\mathbf{r}^{k+1}$$

$$\beta^k = \frac{(\mathbf{r}^{k+1})^T \mathbf{z}^{k+1}}{(\mathbf{r}^k)^T \mathbf{z}^k}$$

$$\mathbf{p}^{k+1} = \mathbf{z}^{k+1} + \beta^k \mathbf{p}^k$$

$$k = k+1$$

Go to Step 2

Given below are few of the most commonly used preconditioners.

2.6.1 Diagonal Preconditioner

The simple preconditioner also known as Jacobi acceleration is diagonal scaling

$$\mathbf{B} = \text{diag}(\mathbf{K}) \tag{2.6.4}$$

2.6.2 Symmetrical Gauss-Seidel

In this method the matrix **K** is decomposed as

$$\mathbf{K} = \mathbf{L} + \mathbf{D} + \mathbf{L}^T \tag{2.6.5}$$

where

L is the lower triangular matrix with zero diagonal entries

D is diagonal of **K**

and the preconditioner **B** is defined as

$$\mathbf{B} = \frac{1}{2}(2\,\mathbf{D} + \mathbf{L})\,\mathbf{D}^{-1}(2\,\mathbf{D} + \mathbf{L}^T) \tag{2.6.6}$$

2.6.3 Incomplete Cholesky Factorization

Meijerink and Vander Vorst [25] transformed the system of equations $\mathbf{K}\,\mathbf{u} = \mathbf{f}$ into

$$\mathbf{B}\,\mathbf{z} = \mathbf{r} \tag{2.6.7}$$

where

$$\mathbf{B} = \mathbf{L}_1^{-1}\,\mathbf{K}\,\mathbf{L}_1^{-T} \tag{2.6.8}$$

$$\mathbf{z} = \mathbf{L}_1^T\,\mathbf{u} \tag{2.6.9}$$

$$\mathbf{r} = \mathbf{L}_1^{-1}\,\mathbf{f} \tag{2.6.10}$$

and $\mathbf{L}_1$ is an approximation to the Cholesky factor of $\mathbf{K}$ constrained to have the same sparsity pattern as $\mathbf{K}$.

2.7 Element by Element Methods

A disadvantage with the above methods is that they require the use of the full matrix $\mathbf{K}$ and hence large storage requirements. When $\mathbf{K}$ is obtained from finite element models, Element by Element (EBE) methods provide a way of solving the system of equations without the use of the complete global stiffness matrix at a time. It does not require a global stiffness matrix storage. Only one element matrix is to be formed and stored at one time. For a very large structural problem modeled by finite elements, the number of unknowns (n) to be solved for is very large and storage of the global stiffness matrix may be unmanageable. In the Element by Element method $\mathbf{K}$ is never assembled and it is factorized approximately in terms of $\mathbf{K}^e$, $e = 1, \ldots, \text{nele}$, where nele is the number of elements, and $\mathbf{K}^e$ is the element stiffness matrix.

The global stiffness matrix is the summation of the element stiffness matrices

$$\mathbf{K} = \sum_{e=1}^{nele} \mathbf{K}^e \tag{2.7.1}$$

The Element by Element Method developed by Hughes and co-workers [7,8] uses a preconditioner of the form

$$\mathbf{B} = \mathbf{W}^{1/2}\,\mathbf{C}\,\mathbf{W}^{1/2} \tag{2.7.2}$$

where **W** is a positive definite diagonal matrix also known as the scaling matrix (in the present case it is the diagonal of the global stiffness matrix) and **C** is a function of **K** . It is desirable that for **B** as the preconditioner, it should be as close to **K** as possible.

$$\mathbf{B} \simeq \mathbf{K} \tag{2.7.3}$$

Hence from equation 2.7.2 and 2.7.3 we get

$$\mathbf{C} = \mathbf{W}^{-1/2}\,\mathbf{K}\,\mathbf{W}^{-1/2} \tag{2.7.4}$$

Using equation 2.7.1, equation 2.7.4 can be written as

$$\mathbf{C} = \mathbf{W}^{-1/2}\sum_{e=1}^{nele}(\mathbf{K}^e)\,\mathbf{W}^{-1/2} \tag{2.7.5}$$

adding and subtracting unit matix from (2.7.5)

$$\mathbf{C} = \mathbf{W}^{-1/2}\sum_{e=1}^{nele}(\mathbf{K}^e)\,\mathbf{W}^{-1/2} - \mathbf{I} + \mathbf{I} \tag{2.7.6}$$

$$= \mathbf{W}^{-1/2}\sum_{e=1}^{nele}(\mathbf{K}^e)\,\mathbf{W}^{-1/2} - \mathbf{W}^{-1/2}\sum_{e=1}^{nele}\mathbf{D}^e\,\mathbf{W}^{-1/2} + \mathbf{I} \tag{2.7.7}$$

$\mathbf{D}^e$ = diagonal of $\mathbf{K}^e$

$$\mathbf{C} = \mathbf{W}^{-1/2}\sum_{e=1}^{nele}(\mathbf{K}^e - \mathbf{D}^e)\,\mathbf{W}^{-1/2} + \mathbf{I} \tag{2.7.8}$$

Defining

$$\tilde{\mathbf{K}}^e = \mathbf{W}^{-1/2}(\mathbf{K}^e - \mathbf{D}^e)\,\mathbf{W}^{-1/2} \tag{2.7.9}$$

we get

$$\mathbf{C} = (\mathbf{I} + \sum_{e=1}^{nele}\tilde{\mathbf{K}}^e) = \mathbf{I} + \tilde{\mathbf{K}} \tag{2.7.10}$$

$\tilde{\mathbf{K}}$ has the same sparsity as $\mathbf{K}$. The goal is to replace the global matrix $\mathbf{K}$ by its element components.

To express $\mathbf{K}$, the global stiffness array as a product of the element stiffness array the following approximation is used

$$\prod_{i=1}^{n}(1+h_i) = (1+h_1)(1+h_2)\ldots(1+h_n) = 1 + \sum_{i=1}^{n} h_i + \text{H.O.T.} \simeq 1 + \sum_{i=1}^{n} h_i \quad (2.7.11)$$

Then $\mathbf{C}$ can be written as

$$\mathbf{C} = \mathbf{I} + \sum_{e=1}^{nele} \tilde{\mathbf{K}}^e \simeq \prod_{e=1}^{nele} (\mathbf{I} + \tilde{\mathbf{K}}^e) \quad (2.7.12)$$

and for each finite element we generate the factorization

$$\mathbf{I} + \tilde{\mathbf{K}}^e = \mathbf{L}_p^e \, \mathbf{D}_p^e (\mathbf{L}_p^e)^T \quad (2.7.13)$$

The matrix $\mathbf{C}$ can be further approximated as

$$\mathbf{C} = \prod_{i=1}^{nele} \mathbf{L}_p(\mathbf{I} + \tilde{\mathbf{K}}^e) \prod_{i=1}^{nele} \mathbf{D}_p(\mathbf{I} + \tilde{\mathbf{K}}^e) \prod_{i=nele}^{1} (\mathbf{L}_p)^T(\mathbf{I} + \tilde{\mathbf{K}}^e) \tag{2.7.14}$$

The factorization of $\mathbf{C}$ is performed completely at the element level. The EBE preconditioners were introduced to make better use of data structure provided by finite element programs.

2.7.1. Cholesky Element by Element Preconditioner

Cholesky factorization is used for a symmetric matrix. In this case the preconditioner is given by

$$\mathbf{B} = \mathbf{W}^{1/2} \prod_{i=1}^{nele} \mathbf{L}_p \prod_{i=nele}^{1} (\mathbf{L}_p)^T \mathbf{W}^{1/2} \tag{2.7.15}$$

where $\mathbf{L}_p$ stands for the lower factor of $\tilde{\mathbf{K}}^e + \mathbf{I}$ and where

$$\tilde{\mathbf{K}}^e = \mathbf{W}^{-1/2}(\mathbf{K}^e - \mathbf{W}^e)\mathbf{W}^{-1/2} \tag{2.7.16}$$

$\mathbf{W}^e$ = diagonal of $\mathbf{K}^e$

Although the element arrays $\mathbf{K}^e$ have the same dimension as the global matrix $\mathbf{K}$, all operations are restricted to the set of equations coupled to the element under consideration.

2.7.2 Crout Element by Element Preconditioner

If $\mathbf{K}$ is not symmetric we can use the Crout EBE preconditioner [8] which is defined by

$$\mathbf{B} = \mathbf{W}^{1/2} \prod_{i=1}^{nele} \mathbf{L}_p \prod_{i=1}^{nele} \mathbf{D}_p \prod_{i=nele}^{1} \mathbf{U}_p \mathbf{W}^{1/2} \tag{2.7.17}$$

where

$\mathbf{L}_p$, $\mathbf{D}_p$ and $\mathbf{U}_p$ stand for the lower, diagonal and upper factors of $\tilde{\mathbf{K}}^e$, and $\tilde{\mathbf{K}}^e$ is the same as in Cholesky's method.

In our present problem though $\mathbf{K}$ is symmetric we use the Crout EBE preconditioner. Actually it is slightly modified to take the symmetry into consideration. It is given as

$$\mathbf{B} = \mathbf{W}^{1/2} \prod_{i=1}^{nele} \mathbf{L}_p \prod_{i=1}^{nele} \mathbf{D}_p \prod_{i=nele}^{1} (\mathbf{L}_p)^T \mathbf{W}^{1/2} \tag{2.7.18}$$

The Crout's preconditioner is a good approximation of $\mathbf{K}$ and shows better convergence for EBE PCG than other type of preconditioners like the diagonal preconditioner.

Chapter 3. Optimization Procedure for Plate with Hole

3.1 Sequential Approximate Optimization

The structural optimization subject to stress and displacements constraints can be written as

minimize S(**X**)

subject to the constraints

$$\tilde{g}_j(\mathbf{u}, \mathbf{X}) \geq 0, \qquad j = 1, \ldots, ng \tag{3.1.1}$$

where S is the objective function of n design variables **X**, and **u** is the displacement vector and $\tilde{g}_j$ are constraint functions. The displacement vector must satisfy the equilibrium equations of the structure given by

$$\mathbf{K}\,\mathbf{u} = \mathbf{f} \tag{3.1.2}$$

where **K** and **f** are the stiffness matrix and the force vector respectively. After substituting **u** into the constraint equations we have

$$g_j(\mathbf{X}) = \tilde{g}_j(\mathbf{X}, \mathbf{u}(\mathbf{X})) \tag{3.1.3}$$

One common procedure to deal with such problems is to use the derivatives of the structural response to form approximate constraints and guide the optimization search toward the solution. The approximate constraints (denoted by subscript 'a') are given by the following equation

$$g_{aj}(\mathbf{X}) = g_j(\mathbf{X}_0) + \Delta g_j(\mathbf{X}, \mathbf{X}_0, \frac{\partial g_j}{\partial \mathbf{X}}) \tag{3.1.4}$$

Using a linear approximation equation 3.1.4 becomes

$$g_{aj}(\mathbf{X}) = g_j(\mathbf{X}_0) + \frac{\partial g_j}{\partial \mathbf{X}}(\mathbf{X} - \mathbf{X}_0) \tag{3.1.5}$$

Constraints are approximated using the approximate displacement field. The optimization problem equation 3.1.1 can then be given by

minimize S(X)

such that

$$g_{aj}(\mathbf{X}) \geq 0, \qquad j = 1, \ldots, ng$$

and $|x_i - x_{0i}| \leq e_i, \qquad i = 1, \ldots, n$ (3.1.6)

where e_i's are move limits chosen to guarantee the accuracy of the approximation g_{aj}. The optimum obtained from the solution of equation 3.1.5 is then used as the next $\mathbf{X}_0$ for the approximation, and the process is repeated to convergence. Often the move limits e_i have to be gradually shrunk to prevent oscillations once the neighborhood of the optimum design is reached.

3.2 Integrated Analysis and Approximate Optimization

The method we employ is a modification on Rizk's Single-Cycle approach [11]. In the integrated analysis and design method instead of solving for **u** exactly, we use approximate values of **u** (call $\tilde{\mathbf{u}}$). The approximation $\tilde{\mathbf{u}}$ are easy to obtain if the method to solve for **u** in the system of equations 3.1.2 is an iterative method. The approximation amounts to using a value of **u** obtained in the iterative method without running the method to full convergence. Apart from **u** being approximate the corresponding constraint $\tilde{g}$ is further linearised. Thus in the present method there is an additional level of approximation. Since the analysis phase for the solution of **u** is the most expensive part of the whole structural optimization process, a saving in the analysis part amounts to significant saving in the design process.

In the present problem of stress minimization, the calculation of the values of element stresses involve the solution of equilibrium equation 3.1.2 for each set of design parameters. The derivatives of the element stresses w.r.t. the shape parameters $(\frac{\partial g_j}{\partial \mathbf{X}})$ are found using simple finite difference scheme $(\frac{\partial g_j}{\partial \mathbf{X}} = \frac{\Delta g_j}{\Delta \mathbf{X}})$. The calculation of derivatives requires perturbing the design (shape) parameters. It should be noted here

that the derivatives with respect to the design parameters are calculated in parallel to the analysis problem. In our problem for a certain guess value of **u** , equation 3.1.2 is iterated for N iterations. Stresses are calculated using the apporoximate value of **u** obtained that is $\tilde{\mathbf{u}}$. Then the shape parameters are perturbed and this leads to finite element mesh regeneration (recalculation of the element node positions). Equation 3.1.2. is re-solved using the same initial guess value of **u** that was used for the analysis part and in this case too the analysis solver is run for only N iterations. This way the derivatives are calculated in parallel to the analysis solution. In the next set of analysis calculation the previous analysis set's solution $\tilde{\mathbf{u}}$ is chosen as the guess value for EBE-PCG. For the derivatives too the previous set of displacement solution for each perturbed design is used as guess values for each EBE-PCG solution for next set of perturbed designs respectively. Fig. 2 shows how the derivatives are calculated in parallel that is, at the same iteration count for both runs of the equilibrium equations. For a case of 'nr' shape parameters the equilibrium equation 3.1.2 has to be solved 'nr+1' times and each time the iterative solver of the linear equation is run to a maximum of N iterations (N is much less than the number of iterations required for complete convergence).

In terms of the traditional nested approach, the inner loop consists of the solution of equation 3.1.2 for each set of shape parameters while the outer loop consists of resizing shape parameters using linear programming. The solution for displacements in the inner loop uses the iterative EBE PCG scheme. Crout's modified preconditioner is used in this example. An iterative scheme is well suited for the problem due to the poor bandedness of the linear system arising from the choice of 3-dimensional elements. The EBE method of PCG is suitable for a problem with large number of variables.

The particular value of N we consider varies from the number of iterations required for full convergence to 1/10th of that number. The set of displacements obtained before resizing the shape parameters are used as the starting values for the EBE PCG scheme. The same holds for finding the derivatives of element stresses with respect to shape parameters. It should be noted here that once the shape parameters have been resized after the optimization, the node coordinates have also changed. Since we allow only small changes in the shape parameters, the previous set of displacements, still approximates the displacements for the nodes for the new mesh. Hence, the use of previous mesh's displacements serves as a good starting point for the next set of EBE PCG iterations. It was observed that with such a scheme, the number of iterations required for convergence to true displacements also decreased substantially as the outer loop proceeded, confirming that the previous displacements are good approximations to the displacements for the new mesh at each step. Fig. 3 shows a flow chart of the method discussed above.

3.3 Hole Shape Optimization Problem

The shape optimization problem considered here is to determine the shape of the central hole in a plate subjected to uniaxial loading as to minimize the stress concentration in the plate. Fig 4 shows the square plate with a central hole subjected to uniform loading. The plate is modelled by 3 dimensional finite elements, see Fig. 5. Only a quarter of the plate is considered because of symmetry and appropriate boundary conditions are applied. (Fig. 5 shows only a 2-d plot of the mesh. There is one layer of elements in the thickness direction). The shape of the hole is approximated by a cosine series. The boundary of the hole is represented by the equation

$$R = \sum_{i=1}^{nr} R_i \cos^{i-1}\theta \qquad (3.3.1)$$

where

nr = number of terms in the series

R_i = coefficients in the series (design parameters)

θ = polar angular co-ordinate of the point on the boundary with origin at center of the plate

Though we assume a certain equation for the hole boundary for exposition of the method, the method presented here is independent of the shape of the hole and can be used for any of the classes of hole shapes.

In terms of finite elements, the problem is to determine $\mathbf{R}'_i$ s (i = 1,nr) so as to minimize the maximum of the stresses in the elements of the plate. Let **R** represent the set of design variables $[R_1, \ldots, R_{nr}]$, nele the number of elements in the plate and σ_{von}(i) the stress in the *i*th element of the plate. The optimization function then is given by

min S (**R**)

subject to

$$S(\mathbf{R}) \geq \sigma_{von}(i, \mathbf{R}) \qquad i = 1, \ldots, nele \qquad (3.3.2)$$

$$G(\mathbf{R}) \geq 0$$

σ_{von} is the Von Mises stress in a element and is given by the equation

$$2\sigma_{von}^2 = \sigma_1^2 + \sigma_2^2 + \sigma_3^2 \tag{3.3.3}$$

where $\sigma_1, \sigma_2, \sigma_3$ are the principal stresses in the element, which are the eigenvalues of the stress tensor σ for the element [26]. The stress in an element is calculated at a gauss point close to the hole boundary, which is used in the Gauss Quadrature method of evaluating a definite integral while calculating the stiffness matrix [27]. The stress tensor for an element is a function of the coordinates of the element nodes and their displacements. As the stress concentration is largest near the hole, only elements at the boundary of the hole are considered for minimizing the maximum value of stress in the plate.

G(**R**) denotes practical constraints on the shape parameters discussed below. One set of constraints guarantees a minimum hole radius ro, by requiring that the distance of any point on the hole boundary from the center of the hole must be at least ro. This constraint is applied at 'nnb' values of θ, where nnb denotes the number of nodes on the hole boundary and θ is the angle of the nodes on the hole boundary from the centre of the plate.

$$\sum_{j=1}^{nr} R_j \mathrm{Cos}^{j-1}\theta_i < \mathrm{ro} \qquad i = 1, \ldots, \mathrm{nnb} \qquad (3.3.4)$$

Another constraint was used to prevent the hole shape from becoming very elongated. It takes the form of

$$\sum_{j=2}^{nr} R_j < 0.9 R_1 \qquad (3.3.5)$$

The move limit constraints limit the absolute change in the radii to be smaller than the maximum of 10 % of the radius and some increment ("vinc") supplied to the optimization routine. Introducing the variable "vinc" allowed the radii to change when their value was very small. The value of "vinc" was decreased for each subsequent optimization step so as not to allow the optimization to oscillate between multiple optima. The above constraint is given by

$$|\Delta R_j| \leq \max(\mathrm{vinc}, 0.1\ R_j) \qquad j = 1, \ldots, \mathrm{nr} \qquad (3.3.6)$$

The above linearised optimization problem can be written as

min S (**R**)

subject to

$$\sigma_{von}(i,\mathbf{R}_0) + \sum_{j=1}^{nr} \frac{\partial \sigma_{von}(i,\mathbf{R})}{\partial \mathbf{R}_j} \Delta \mathbf{R}_j \leq \mathrm{S}(\mathbf{R}) \qquad \mathrm{i} = 1, \ldots, \mathrm{nele}$$

$$\sum_{j=1}^{nr} \mathrm{R}_j \mathrm{Cos}^{j-1}\theta_i < \mathrm{ro} \qquad \mathrm{i} = 1, \ldots, \mathrm{nnb}$$

$$\sum_{j=2}^{nr} \mathrm{R}_j < 0.9\mathrm{R}_1$$

$$|\Delta \mathrm{R}_j| \leq \max(\mathrm{vinc}\ , 0.1\ \mathrm{R}_j) \qquad \mathrm{j} = 1, \ldots, \mathrm{nr}$$

This problem is solved using the IMSL subroutine ZX4LP, which solves the linear programming problem via the Simplex algorithm.

Chapter 4. Results and Discussions

4.1 Introduction

We present results of the Integrated Analysis and Design approach as applied to the hole shape optimization. We validate our stress analysis implementation against a standard finite element program. We check our optimization procedure for a particular hole radius and plate ratio against the experimental results published earlier for the same problem. We present the optimal hole shape obtained by the integrated design and compare the integrated approach against the sequential optimization approach.

4.2 Validation of the Finite Element Model

We verified our analysis and design implementation by cross checking the stress values in the mesh elements against those generated by the EAL program [28] for the same mesh and uniform loading of the plate. The plate data and mesh discretization are given in Table 1 and Fig. 6 respectively. The stresses for two elements on and near the boundary are given in Table 2. Though the numerical values are different between the

two programs, their magnitudes are comparable. The difference occurs due to different finite element formulations and the difference in the points at which the stress is calculated. While we use the Gauss quadrature point (-0.5773503, -0.5773503, 0.0), nearest to hole boundary, for calculating stresses, EAL calculates it at the nodes of the element. In view of the fact that the finite element formulations are different between the two cases, the agreement seems reasonable.

Durelli and Rajaiah [19] presented experimental stress concentration results using photoelasticity for optimized hole shapes in a finite plate for different ratios of the diameter of the hole to the width of the plate. They also presented the stress concentrations at the boundary of the circular hole. We compared the stress concentration results through our implementation against those in [19] for a particular value of hole diameter to plate width ratio (D/W) of 0.42 [Table 3] and [Fig. 5]. Stress concentration is calculated as the ratio of the maximum stress and the applied stress. For the case considered the maximum stress concentration found is 4.774 against the experimental result of 4.913, leading to the acceptable error of 2.87 % . This verifies our finite element model.

4.3 Validation of the Optimization Procedure

We compared the optimal shape achieved by the integrated analysis and design process for the central hole in a plate with that presented in [19]. Since the hole radius in [19] is constrained to be constant at the edges of the quarter plate, we added similar constraints to the optimization problem to get meaningful comparisons. The test problem and the mesh data are given in Fig. 5 and Table 3, respectively. The final shape of the optimized hole is compared against that presented by Durelli and Rajaiah [Fig. 7]. The EBE PCG

scheme was run to full convergence and the hole shape ($\sum_{i=1}^{nr} R_i \cos^{i-1}\theta$) was optimized for two values of *nr* (nr = 4 and nr = 5). As can be seen, our design has shape similar to the design in [19]. As expected, the higer the value of *nr*, the better is the approximation of an arbitrary curve through the hole shape for our design. Increasing *nr* yields optimal curves through our approach that are closer to the optimal curve presented in [19]. We expect our method to approach the Durelli curve for higher values of *nr* .

4.4 Derivative Convergence

As explained earlier, the outer loop in the present approach performs an optimization to update the values of the design parameters. The optimization uses a linear approximation of the stresses with respect to the design parameters. In order that the optimization procedure converge, the derivatives must closely approximate the actual derivatives of the Von Mises stress with respect to the design parameters. Since the derivatives are calculated using the finite difference scheme, stresses for the initial design and the perturbed design have to be calculated. The stresses in the integrated approach are found using the displacements calculated by incomplete convergence of the EBE PCG scheme. But how *incomplete* a convergence is required for acceptable derivatives must be investigated. The more *incomplete* the EBE PCG convergence one can get away with, the lower is the cost of the design process.

We plot the derivatives of the Von Mises stress with respect to the design parameters of a boundary element as a function of the number of iterations of EBE PCG convergence [Fig. 8]. The full convergence of the EBE PCG scheme for the problem [Table 3] with 1492 degrees of freedom requires 147 iterations (NMAX). We vary the value of the number of iterations (N) allowed for the EBE PCG scheme from 10 to 150

(> NMAX), considering the derivatives to be accurate for the full convergence case (NMAX). For $N > 32$ all the derivatives have the correct sign. Some derivatives for $N < 32$ have the wrong signs. This suggests that a choice of $N < 32$ may lead to bad derivative approximations and design updates. In such a case, the integrated approach may fail to converge to the optimal solution. Indeed the results presented next show that the choice of $N < 32$ is a poor choice and shows very poor convergence to the optimal hole shape.

4.5 Optimization Results

We present the results of the integrated analysis and design for the optimal central hole shape in a finite plate. The problem specifications are the same as Table 3. The maximum number of iterations for EBE PCG was varied from 20 to full convergence (NMAX = 147). The outer loop of optimization step was iterated until full convergence.

The final hole shape design for $N = 40$ and $N = NMAX$ converged to very similar shapes [Fig. 9] demonstrating the feasibility of integrating the analysis and design in the sequential approximate optimization. The number of EBE PCG iterations [Table 5a & 5b], required for the complete design (which included those required for calculating derivatives) shows a saving of 32 % for $N = 40$ over the full EBE PCG convergence method while the maximum stress concentration for the two cases agree to within 0.28 % . The optimal hole shapes are shown in Fig. 9 and the mesh discretization for the final hole shape is shown in Fig. 10. The final hole shape shows a decrease in stress concentration of 26.4 % over the initial design of the circular hole. The optimum hole shape looks like an ellipse with the hole width having the minimum hole radius allowed

(0.5 in.) in the problem. The stress concentration at the hole boundary is shown in Fig. 11.

As the optimization proceeds with updated designs at each step, the total number of iterations required for full EBE PCG convergence comes down from 147 down to 60 and is occasionally less than 60. This is because at each step of the integrated analysis and design the displacements used for the EBE PCG scheme are the displacements calculated at the previous step for the previous design. The closer are the initial guess values to their correct values, the faster is the convergence in iterative methods. The decrease in the number of EBE PCG steps shows that the guess values are good approximations to their real values for the particular design. Such a behaviour is characteristic of a smooth convergence to the optimal result at each step of the optimization.

Choosing $N = 30$ showed a very slow convergence to the solution, while the choice of $N = 20$ diverged away from the solution. The results seem consistent with the analysis of the derivatives presented earlier for different numbers of EBE PCG iterations that suggested the use of $N > 32$ for convergence. The variations in the maximum stress concentration in the plate are plotted against the number of outer optimization steps in Fig. 12. The graphs show that as the number of iterations for EBE PCG decreases, the integrated analysis and design shows slower convergence. The similar graph for $N = 20$ is not meaningful to present because the stresses are calculated using the displacements which may not even be close to their real solutions. The best choice of N for our problem seems to be close to 35.

In the present scheme, a new hole shape design requires rediscretization of the mesh. This leads to the recalculation of the forces acting at each element using the uniform loading after each design update. Since the forcing function affects only the outer

boundary elements of the plate and the change in the hole shape has very little effect on the outer boundary element dimensions, we experimented with keeping the forcing function the same across the iterations. This removes the effect of the changes in the element forces on their displacements due to redesign and hence shows better design convergence. Results using the inexact forces in the elements (calculated only once for the initial mesh discretization) are presented in Table 4b. It is not surprising that the optimal shape of the hole converged to the same results as for using the exact forces in elements at each redesign step see Fig. 13 and the the stress concentration for optimum design is the same Fig. 14. The convergence is better than using the exact forces and saved 15 % EBE PCG iterations over its exact force counterpart using full EBE PCG convergence [Table 5b]. The above scheme is an example of another kind of approximation that can be used in the design phase.

4.6 Multiple Layers

The program for the single layer case was extended to include more than one layer of elements along the thickness (z) direction. The results of the finite element procedure used in the present study are first validated against the EAL analysis program [28] with two layers of elements. The average stress results [Table 6] obtained by the EAL program and the EBE-PCG are comparable. For both cases the stresses are calculated at element position A [Fig. 5]. The point at which the stresses are found is at half the thickness from the bottom of the plate. Table 6 also compares the average stresses at the centre of the plate for the same element position for one layer case in z-direction and it can be seen that they compare well with the two layer case.

The hole shape optimization problem for a plate with the same thickness was solved for the one and two elements cases along the z-direction. The analysis was done to full convergence at each step. It can be seen from the Fig. 15 that the optimum hole shape for both the cases are very close. We observed that the analysis phase for the two layer case converged in less number of iterations as compared with the single layer case, but it must be noted that the number of operations at each iteration for the two layer case increases as the total number of elements in the plate doubles. The ratio of the operation count for one full analysis between the two element and the single element case turned out to be 1.06. Considering a direct method, banded systems LDL^T solver, the operation count for two layer case is nearly three times the single layer case. We expect that using multiple elements in the z-direction will have good convergence properties and will be more efficient than the corresponding direct method solvers, as the sparse matrices generated by multiple elements get less structured. We still have to investigate further on the above methods to be able to make fair comparisons. The integerated analysis and design technique can be used to determine optimum hole shape for thick plates, which can be modelled by more than one element in the thickness direction and this can be extended to analyse and optimize layered composite plates.

Chapter 5. Conclusions

When structural analysis is performed via iterative solution technique it is possible to integrate the analysis and design iterations in an integrated analysis and design procedure. The integrated analysis and design approach due to Rizk was applied to the problem of hole shape optimization in thick plates.

The plates were modeled by three dimensional eight noded elements. An element by element (EBE) preconditioned conjugate gradient (PCG) method was used for the structural analysis, because this method is well suited for poorly banded three dimensional problems. The plates were optimized so as to minimize the stress concentration near the hole measured by the ratio of the Von Mises stress to the applied boundary stress. The analysis program was validated by comparision to a commercial finite-element program as well as photoelastically obtained stress concentrations. Similarly, the optimization procedure was checked against plates optimized by a photoelastic technique. Good agreement was observed.

The integrated analysis and design approach tested here is based on partially converged solutions of the EBE-PCG iterative process. A study of the effect of the number of iterations on analysis and derivative accuracy was performed. Based on this analysis a choice was made for the number of iterations to be used in the integrated analysis and design procedure. It was found that the cost of the design could be significantly reduced with only minimal effects on the final shape and stress concentration factor.

List of References

1. Haftka, R.T. and Kamat, M.P., "Elements of Structural Optimization ", Martinus Nijhoff, The Netherlands, 1985.

2. Fox, R.L. and Schmit, L.A., "Advances in the Integrated Approach to Structural Synthesis ", Journal of Spacecraft and Rockets, Vol. 3, 1966, pp. 858-866.

3. Schmit, L.A., Bogner, F.K. and Fox, R.L., "Finite Deflection Discrete Element Analysis Using Plate and Shell Discrete Elements ", AIAA Journal, Vol. 6, 1968, pp. 781-791.

4. Fox, R.L. and Stanton, E.L., "Developments in Structural Analysis by Direct Energy Minimization ", AIAA Journal, Vol. 6, 1968, pp. 1036-1042.

5. Fox, R.L. and Kapoor, M.P., "A Minimization Method for the Solution of Eigenproblem Arising in Structural Dynamics " Proceedings of the Second Conference on Matrix Methods in Structural Mechanics, Wright-Patterson AFB, Ohio, AFFDL-TR-68-150.

6. Kamat, M.P. and Hayduk, R.J., " Recent Developments in Quasi-Newton Methods for Structural Analysis and Synthesis ", AIAA Journal, Vol. 20, 1982, pp. 672-679.

7. Hughes, T.J.R., Levit, I. and Winget, J.M., "An Element-by-Element Solution Algorithm for Problems of Structural and Solid Mechanics ", Computer Methods in Applied Mechanics and Engineering, Vol. 36, 1983b, pp. 241-254.

8. Hughes, T.J.R., Levit, I., Winget, J.M. and Tezduyar, T., "New Alternating Direction Procedures in Finite Element Analysis Based upon EBE Approximate Factorizations ", (S.N.Atluri and N.Perrone, editors), Computer Methods for Nonlinear Solids and Structural Mechanics, AMD-Vol. 4, 1983c, pp. 75-109.

9. Haftka, R.T., "Simultaneous Analysis and Design ", AIAA Journal, Vol. 23, July 1985, pp. 1099-1103.

10. Haftka, R.T. and Kamat, M.P., "Simultaneous Nonlinear Structural Analysis and Design ", to be published in Computational Mechanics.

11. Rizk, M.H., "The Single-Cycle Scheme - A New Approach to Numerical Optimization ", AIAA Journal, Vol. 21, Dec. 1983, pp. 1640-1647.

12. Haftka, R.T., "Integrated Nonlinear Structural Analysis and Design ", Proceedings of the AIAA/ASME/ASCE/AHS Structures, Structural Dynamics and Materials Conference, Williamsburg, Virginia, Vol. 3, April 1988, pp. 1324-1332.

13. Michell, A.G.M., "The Limits of Economy of Material in Frame-Structures ", Phil. Mag. 8, 1904, pp. 589-597.

14. Pragner, W., "Optimal Layout of Trusses with Finite Number of Joints ", Journal of Mechanics Physics Solids, Vol. 26, 1978, pp. 241-250.

15. Strang, G. and Kohn, R.V., "Hencky-Prandtl Nets and Constrained Michell Trusses ", Proceedings of International Symposium on Optimal Structural Design, Tucson, Arizona, 1981, pp. 4-17 - 4-22.

16. Rozvany, G.I.N., "A General Theory of Optimal Structural Layouts ", Proceedings of International Symposium on Optimal Structural Design, Tucson, Arizona, 1981, pp. 4-37 - 4-45.

17. Botkin, M.E., "Shape Optimization of Plate and Shell Structures" AIAA Journal, Vol. 20, 1982, pp. 268-273.

18. Durelli, A.J. and Rajaiah, K., "Optimum Hole Shapes in Finite Plates Under Uniaxial Load ", Journal of Applied Mechanics, ASME, Vol. 46, Sept. 1979, pp. 691-695.

19. Durelli, A.J., Erickson, M. and Rajaiah, K., "Optimum Shapes of Central Holes in Square Plates Subjected to Uniaxial Uniform Load ", International Journal of Solids and Structures, Vol. 17, 1981, pp. 787-793.

20. Dhir, S.K., "Optimization of Openings in Plates under Plane Stress ", AIAA Journal, Vol. 21, Oct. 1983, pp. 1444-1447.

21. Curtis, J.P. and Walpole, L.J., "Optimization of the Torsional Rigidity of Axysymmetric Hollow Shafts ", International Journal of Solids and Structures, Vol. 18, 1982, pp. 883-887.

22. Rosanoff, R.A. and Webel, H., "On the Convergence Rate of Iterative Methods for the Solution of Positive Definite Linear Equations ", Computer Methods in Applied Mechanics and Engineering, Vol. 7, 1976, pp. 369-375.

23. Golub G.H., and Van Loan C.F., "Matrix Computations ", The John Hopkins University Press, MD, 1987.

24. Hestenes, M.R. and Stiefel, E., "Method of Conjugate Gradients for Solving Linear Systems ", Journal of Research of the National Bureau of Standards, Vol. 49, 1952, pp. 409-436.

25. Meijerink, J.A. and Van der Vorst, H.A., "An Iteration Solution Method for Linear Systems of which the Coefficient Matrix is a Symmetric "M" Matrix ", Mathematics of Computation, Vol. 31, 1977, pp. 148-162.

26. Popov, E.P., "Mechanics of Materials ", Prentice-Hall, India, 1981.

27. Cook, R.D., "Concepts and Applications of Finite Element Analysis ", J.Wiley & Sons, NY, 2nd edition.

28. Whetstone, W. D., " EISI-EAL Engineering Analysis Language Reference Guide ", Engineering Infomation Systems, Incorporated, San Jose, California, 1983.

TABLE 1. Test Data for EAL and EBEPCG Stress Comparison

Material	Aluminium
Dimensions of the Plate	10 x 10 x 0.1 in.
Radius of the initial hole	0.375 in.
Young's Modulus E	1.0E+07 psi
Poisson's Ratio	0.25
Applied Load	3000 psi

MESH DATA FOR QUARTER PLATE

Number of elements around the hole boundary	8
Number of nodes	486
Number of elements	209
Number of Degrees of freedom	1458

TABLE 2. Comparison of element stress using EBEPCG and EAL

Element no. - 7 [Fig.6]

	EBE (psi)	EAL (psi)
σ_x	6234.700	6680.700
σ_y	381.860	244.510
σ_z	-55.667	-49.440
τ_{xy}	-1508.100	-1912.300
τ_{yz}	4.720	0.026
τ_{zx}	24.000	-0.980

Element no. - 9 [Fig. 6]

	EBE (psi)	EAL (psi)
σ_x	-116.490	-133.840
σ_y	-1991.800	-1684.300
σ_z	-23.375	-38.382
τ_{xy}	173.400	337.860
τ_{yz}	-0.548	-3.205
τ_{zx}	-1.442	-7.832

TABLE 3. Data for Test Problem

Material	Aluminium
Dimensions of the Plate	2.8 x 2.8 x 0.25 in.
Radius of the initial hole	0.588 in.
Hole Diameter/Plate Width	0.42
Young's Modulus E	1.0E+07 psi
Poisson's Ratio	0.25
Applied Load	3000 psi

MESH DATA FOR QUARTER PLATE

Number of elements around the hole boundary	10
Number of nodes	496
Number of elements	214
Number of Degrees of freedom	1488

TABLE 4a. Comparison of Maximum Stress Concentration (exact force)

Initial design	4.772
Full convergence	3.512
Max. Number of iters. for EBE = 40	3.511
Max. Number of iters. for EBE = 30	3.599

TABLE 4b. Comparison of Maximum Stress Concentration (inexact force)

Initial design	4.772
Full convergence	3.513
Max. Number of iters. for EBE = 40	3.511

TABLE 5a. Comparison of Number of Iters. for Opt. Design(exact force)

Full convergence	5742
Max. Number of iters. for EBE = 40	3900
Max. Number of iters. for EBE = 40	4464
(Full covergence at 1st step)	

TABLE 5b. Comparison of No. of Iters. for Opt. Design(inexact force)

Full convergence	4898
Max. Number of iters. for EBE = 40	3863
Max. Number of iters. for EBE = 35	3897

TABLE 6. Comparison of average element stress using EBEPCG and EAL

(for Plate with 2 elements in Z direction)

Element A - 7 [Fig.5]

	EAL (psi)	EBE (psi)	EBE (psi) (1 ele. along z)
σ_x	14206.50	14039.63	14035.00
σ_y	333.33	302.07	301.92
σ_z	97.27	3.06	-9.25
τ_{xy}	-727.63	-725.28	-723.87
τ_{yz}	-0.24	-0.81	0.78
τ_{zx}	0.46	1.43	-3.32

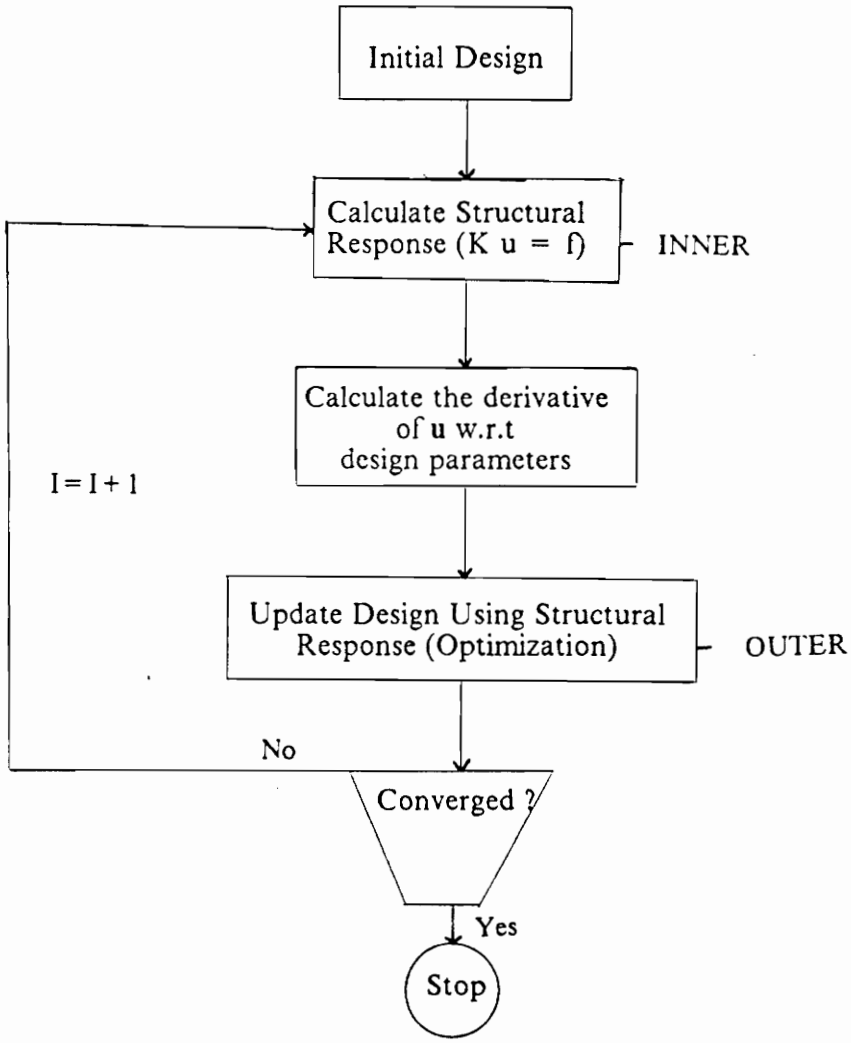

Figure 1. Flow Chart for Nested Approach

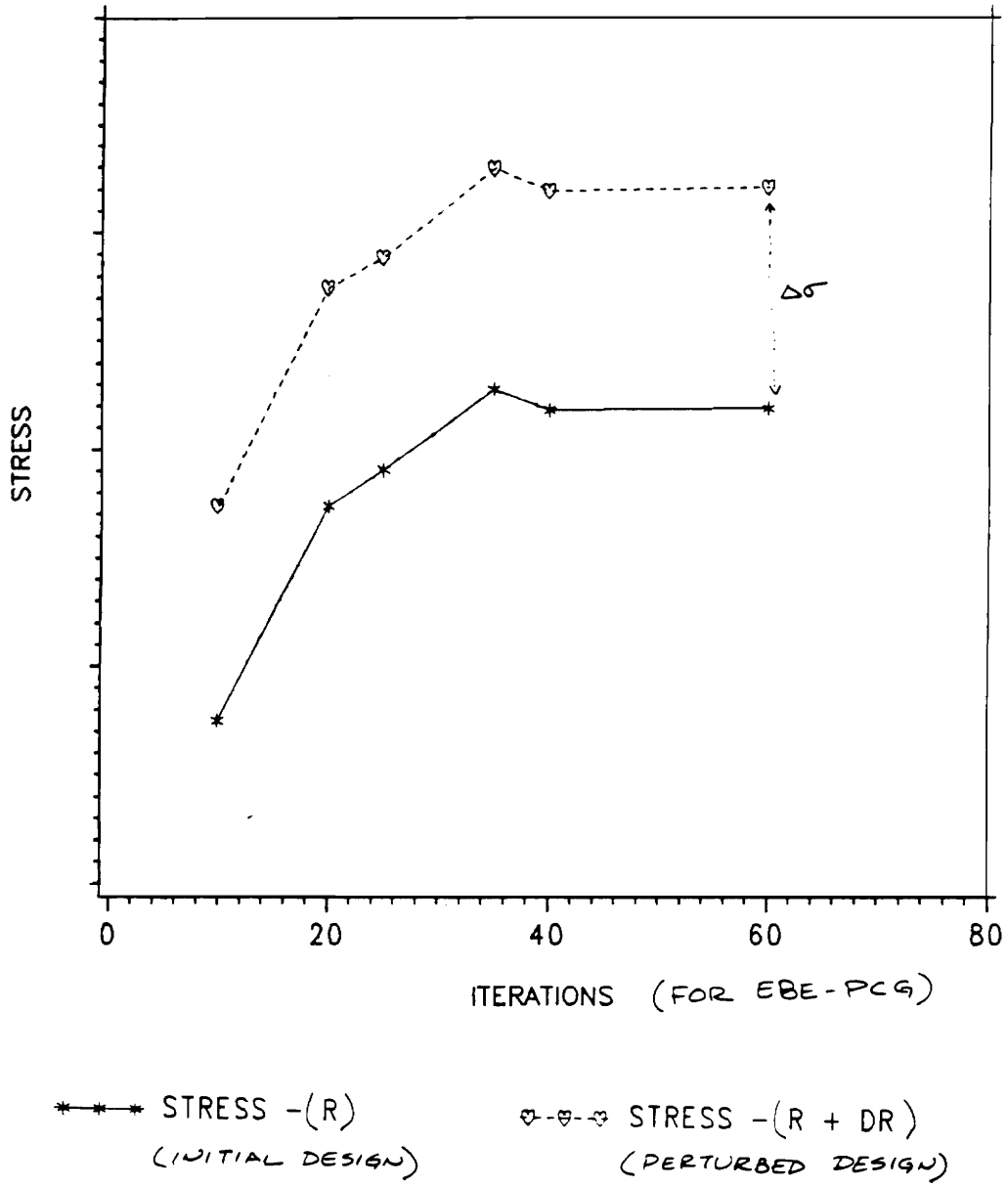

Figure 2. Derivative Calculation : $\frac{\partial \sigma}{\partial r} = \frac{\Delta \sigma}{\Delta r}$

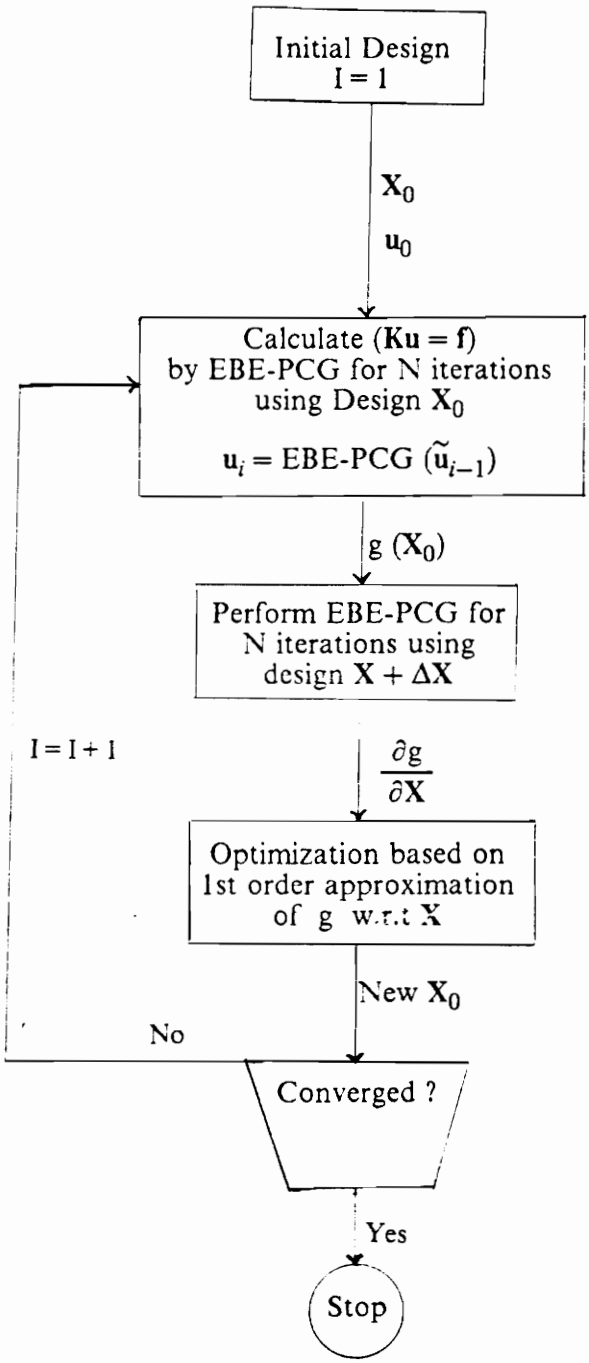

Figure 3. Flow Chart for Integrated Analysis and Design

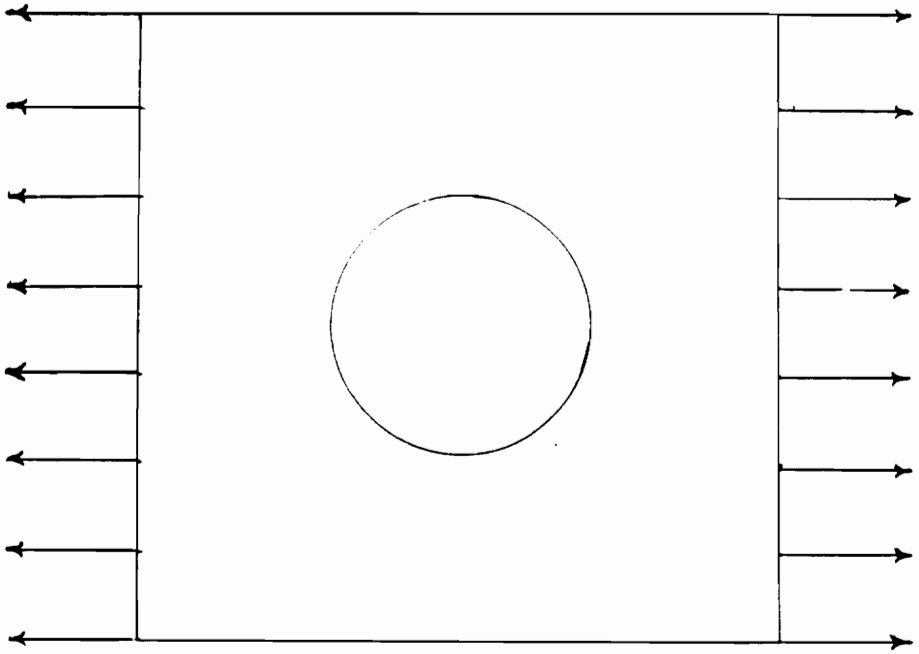

Figure 4. Plate with a Central Hole Subjected to Uniform Loading

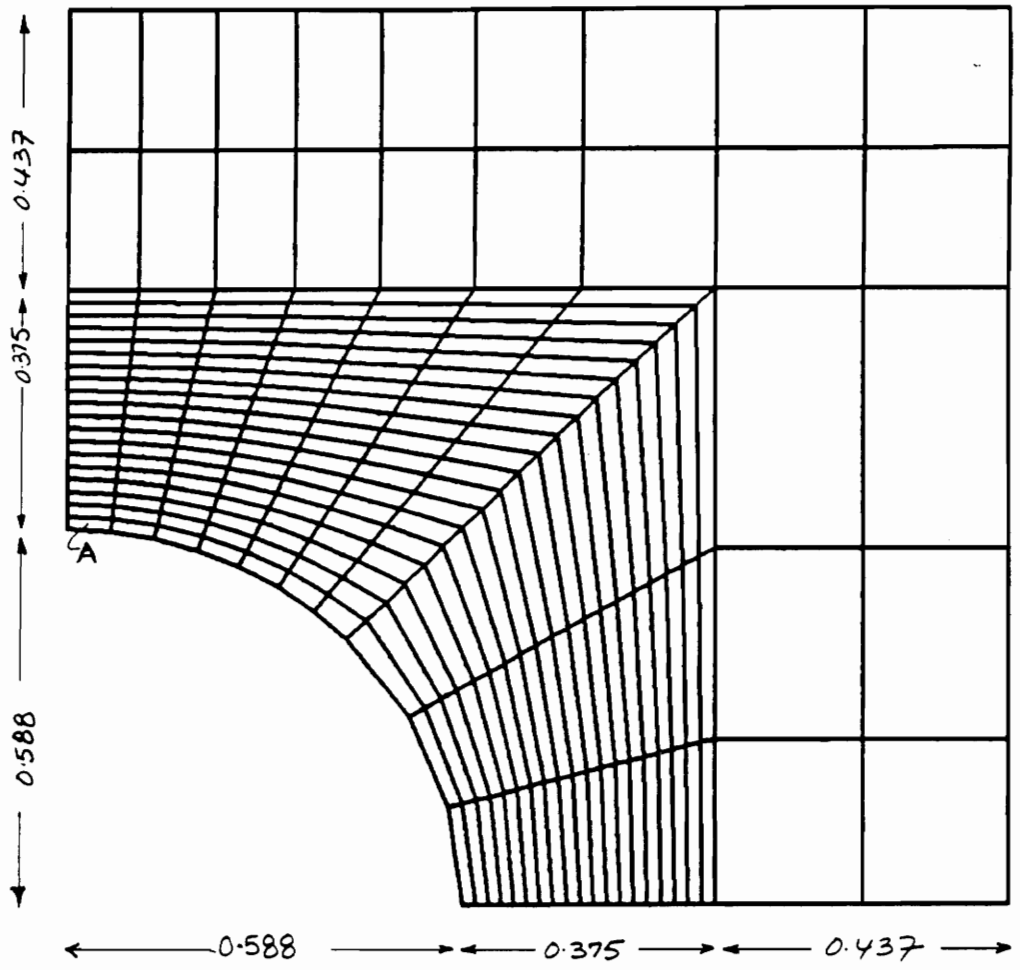

Figure 5. Mesh Discretization - Initial Design

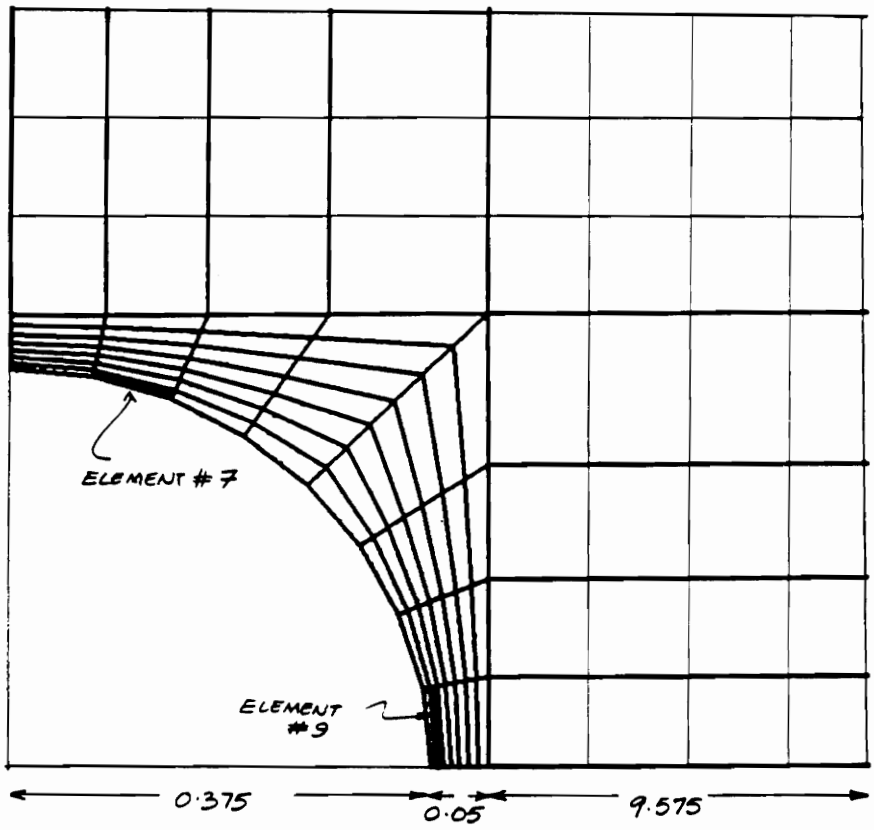

Figure 6. Mesh Used for EBE PCG and EAL Stress Comparison

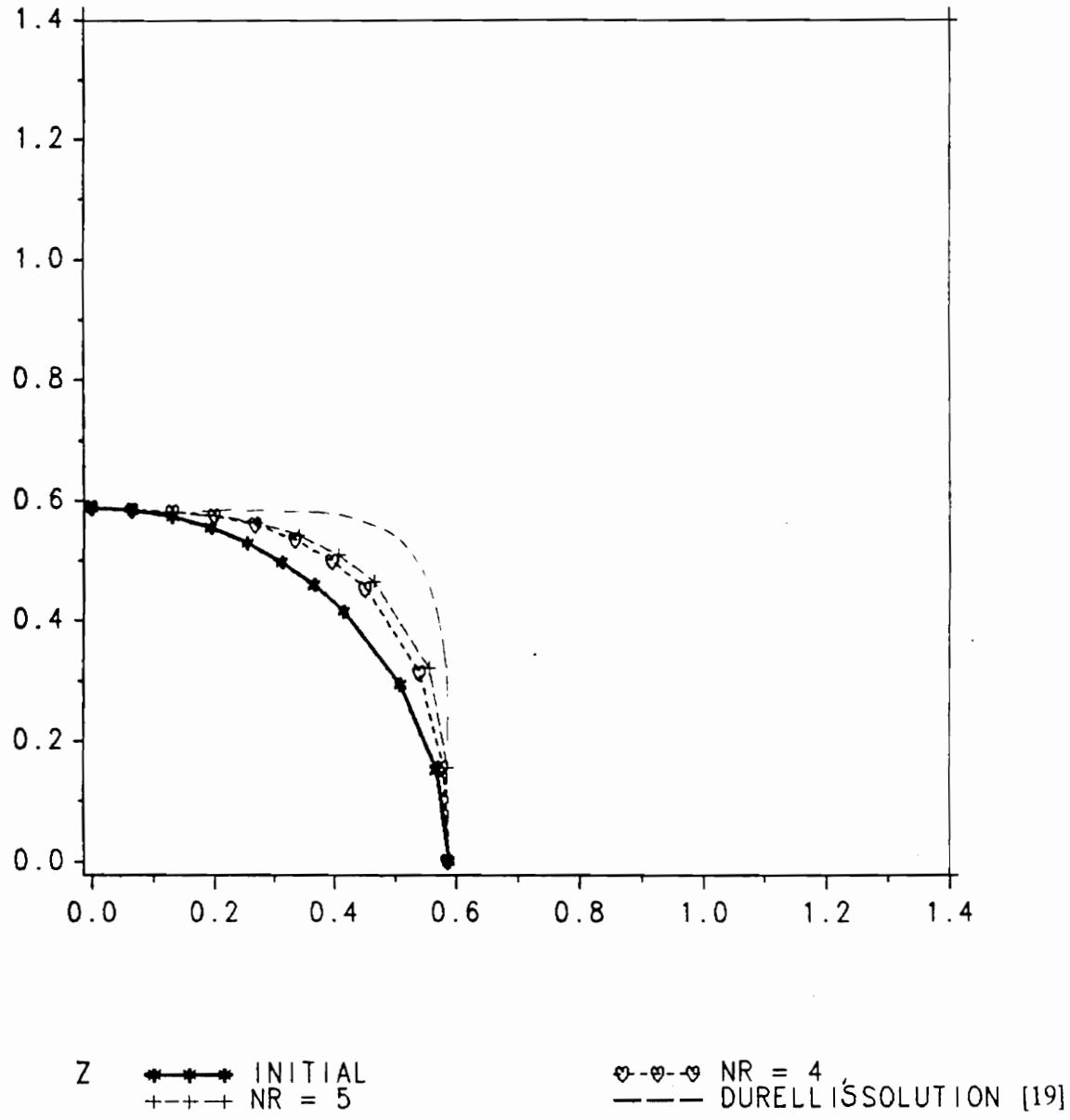

Figure 7. Comparison of Optimal Hole Shape with Durelli's experimental result

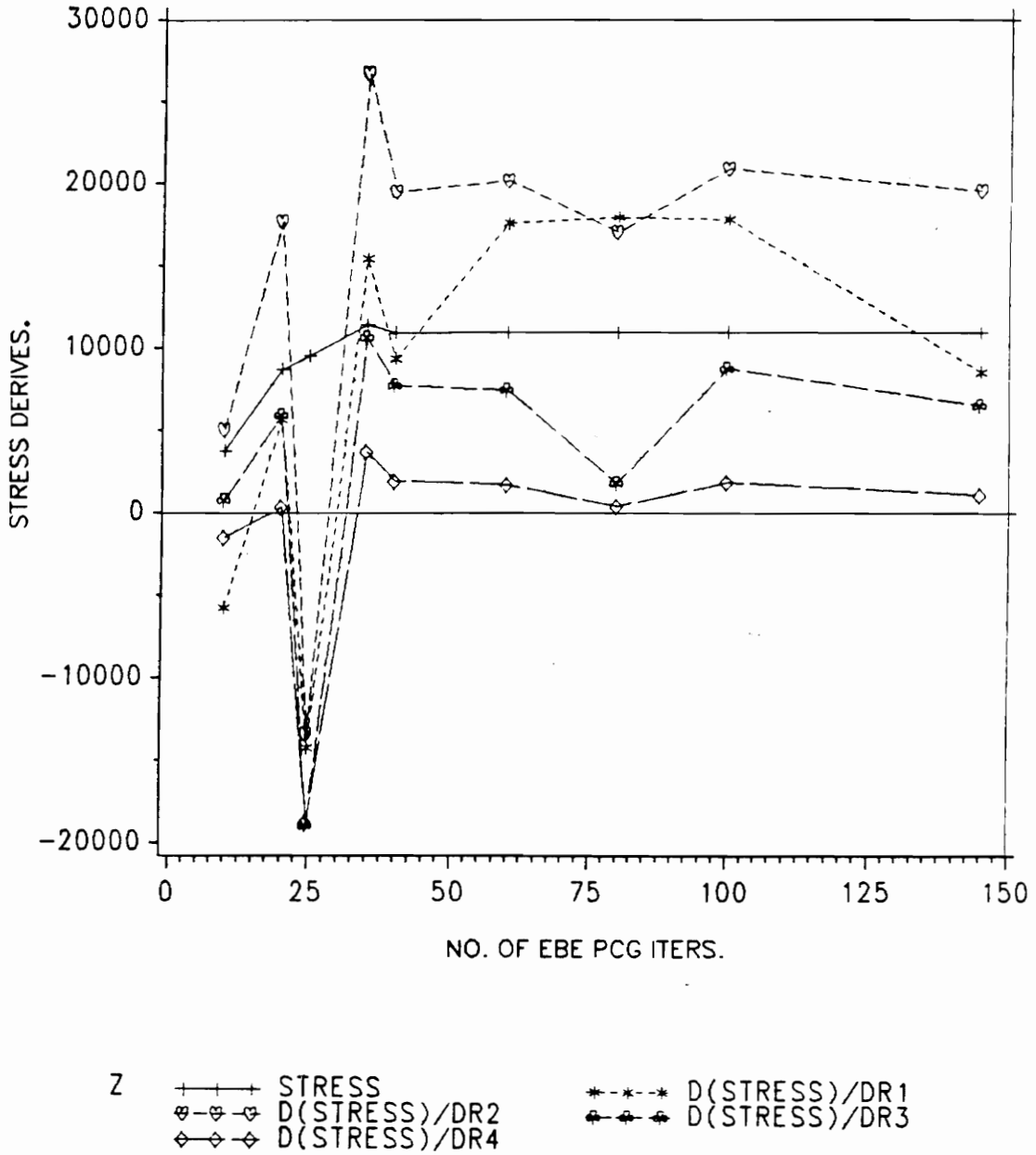

Figure 8. Derivatives of Von Mises stress of element 7 as a function of the number of EBE-PCG iterations

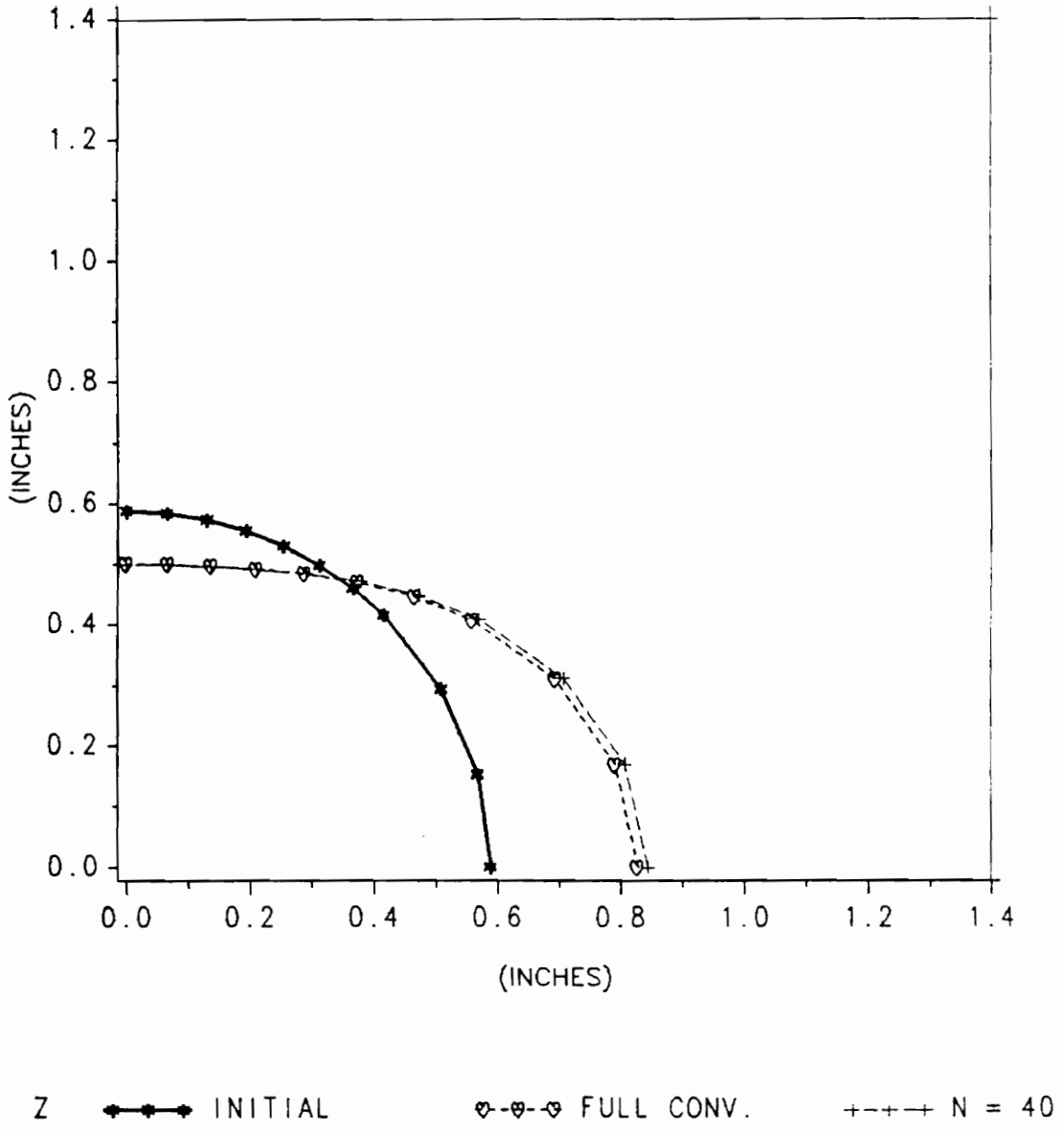

Figure 9. Hole Shapes

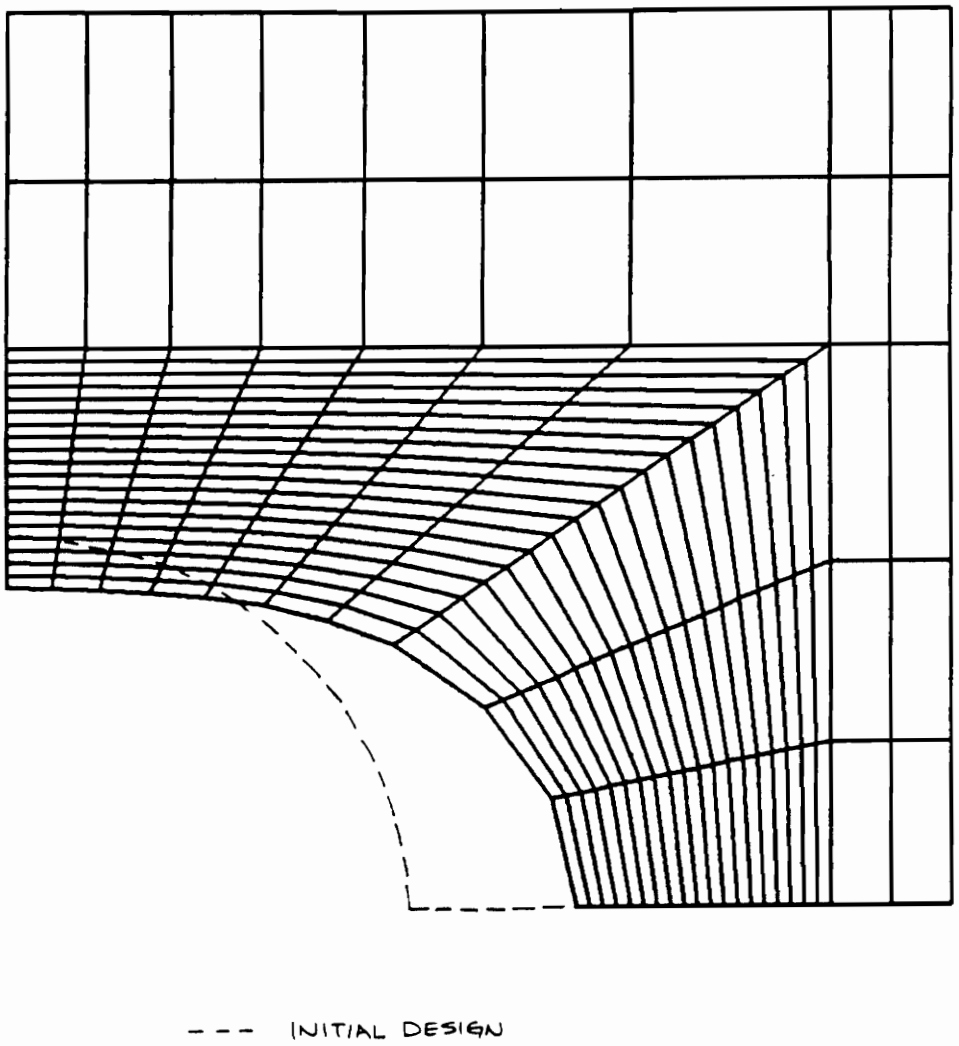

Figure 10. Mesh Discretization for Optimal Hole

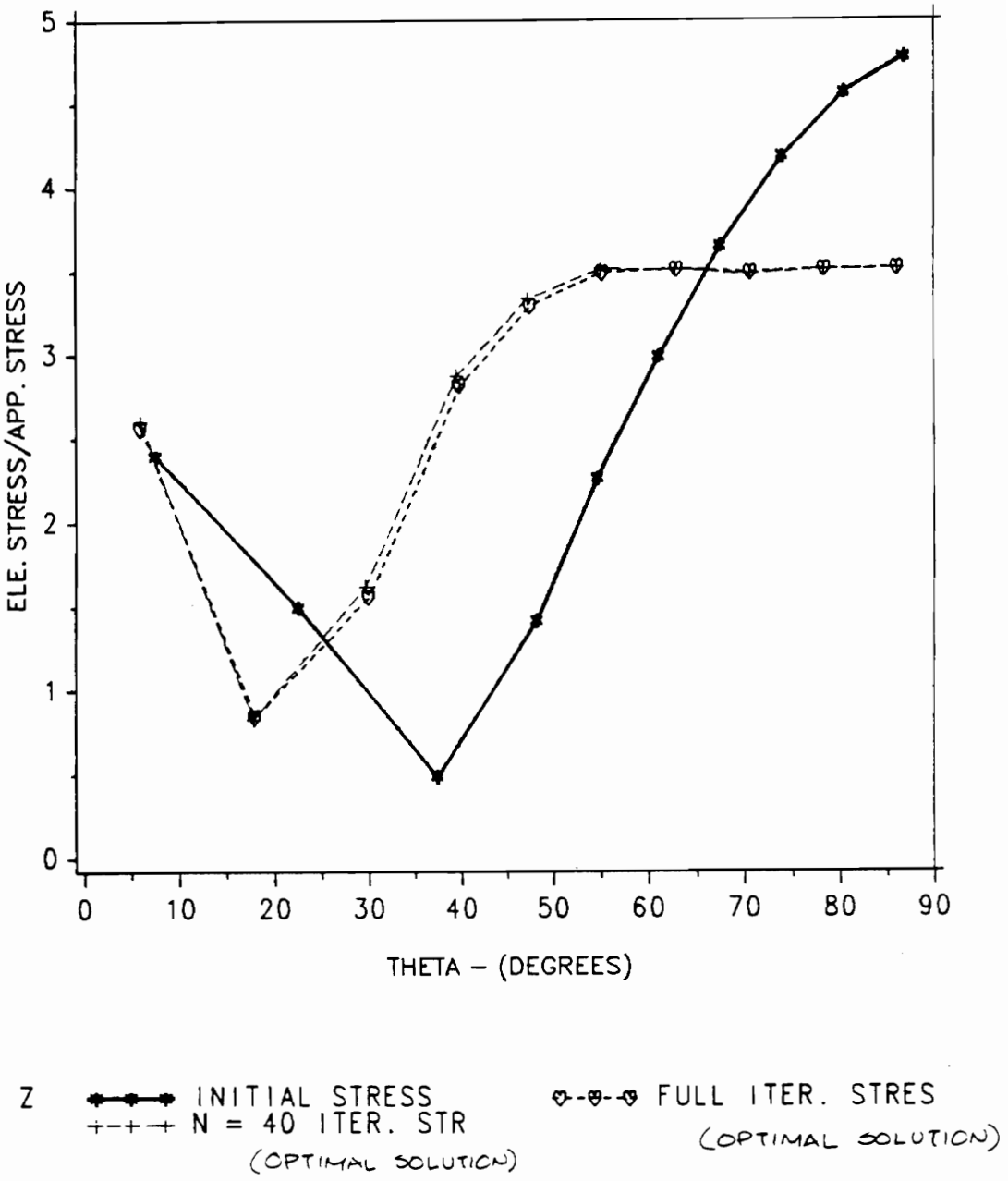

Figure 11. Stress Concentration in Elements around Hole Boundary

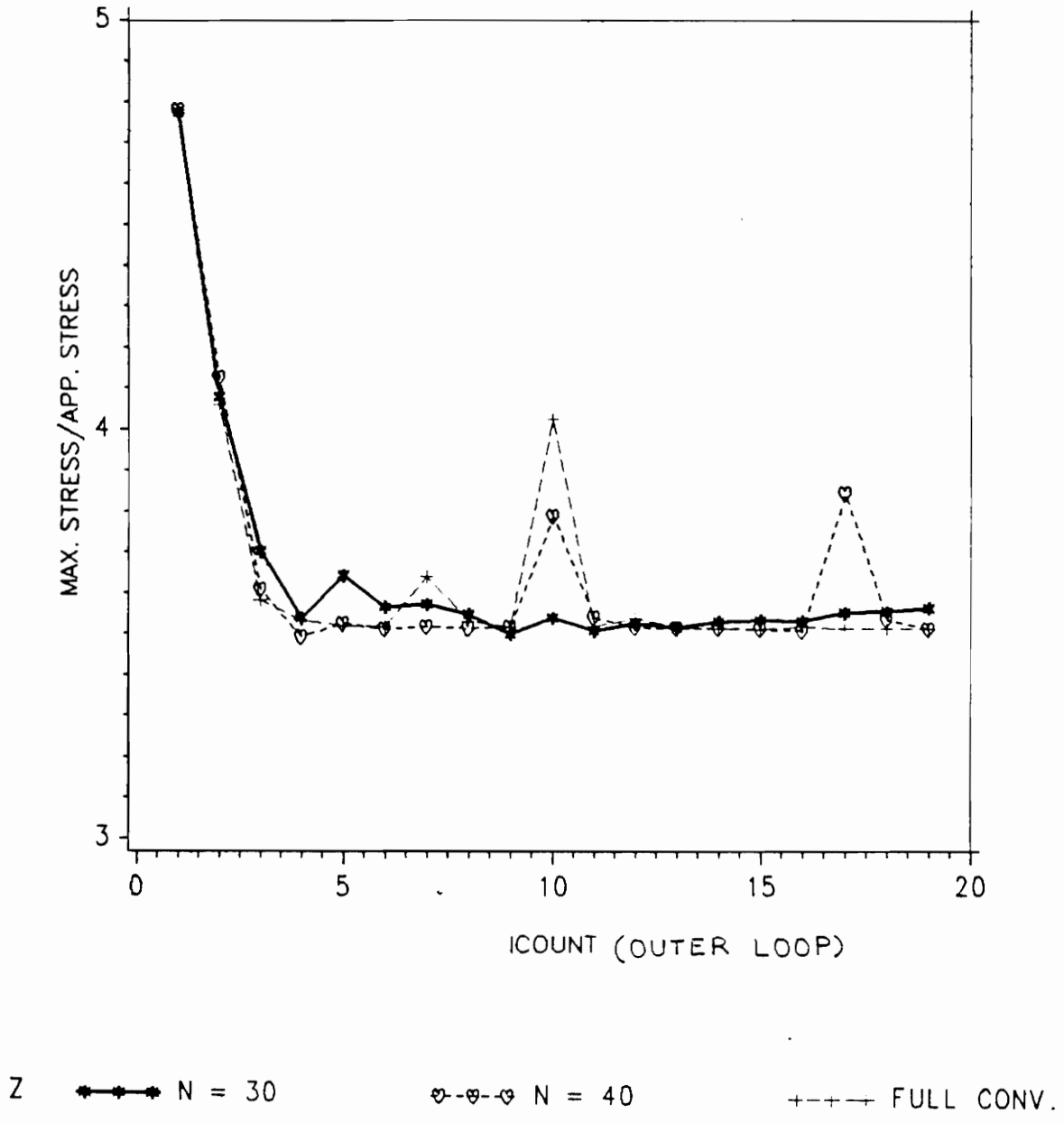

Figure 12. Outer Loops vs Maximum Stress Concentration

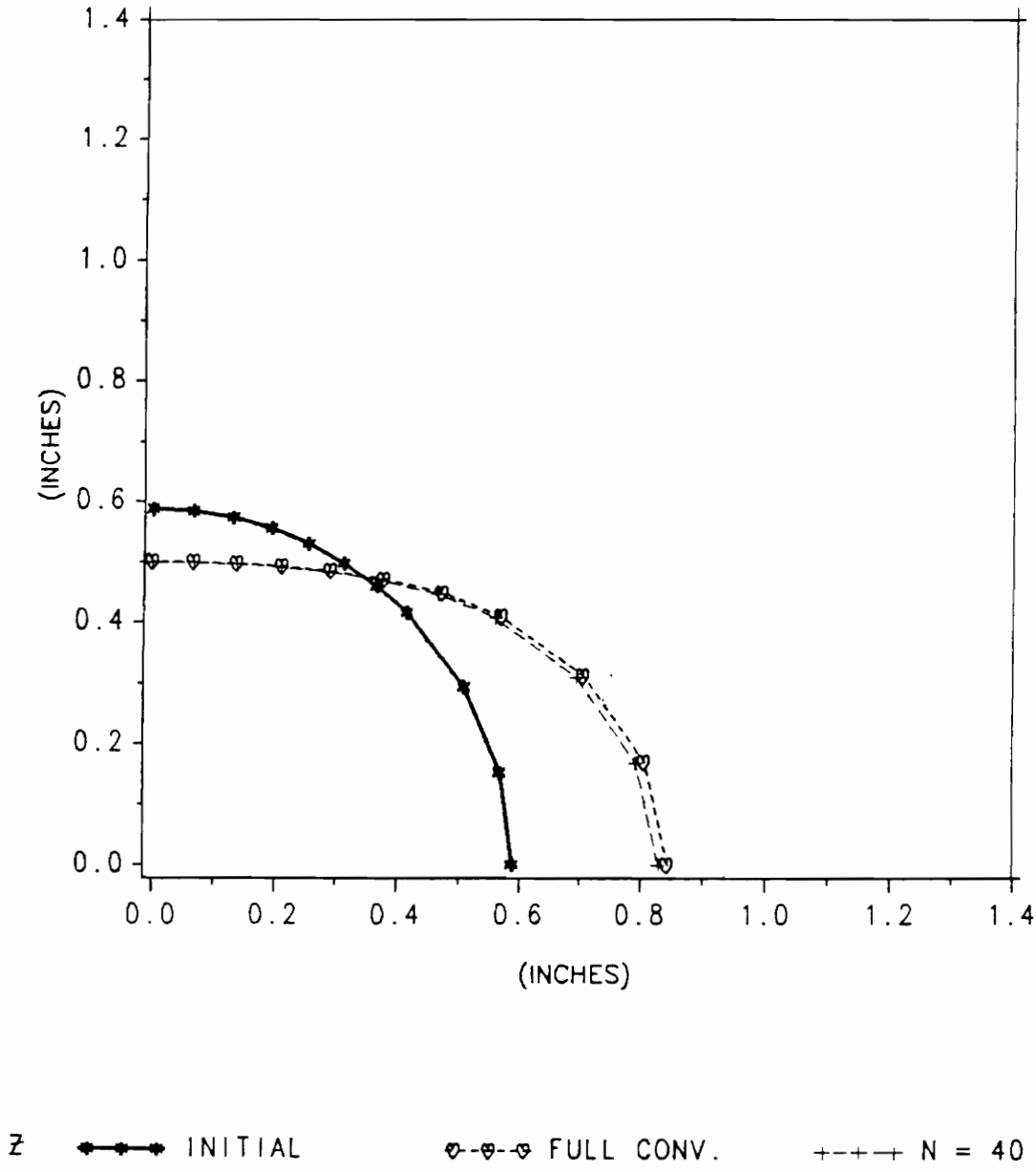

Figure 13. Hole Shapes (Inexact Forces)

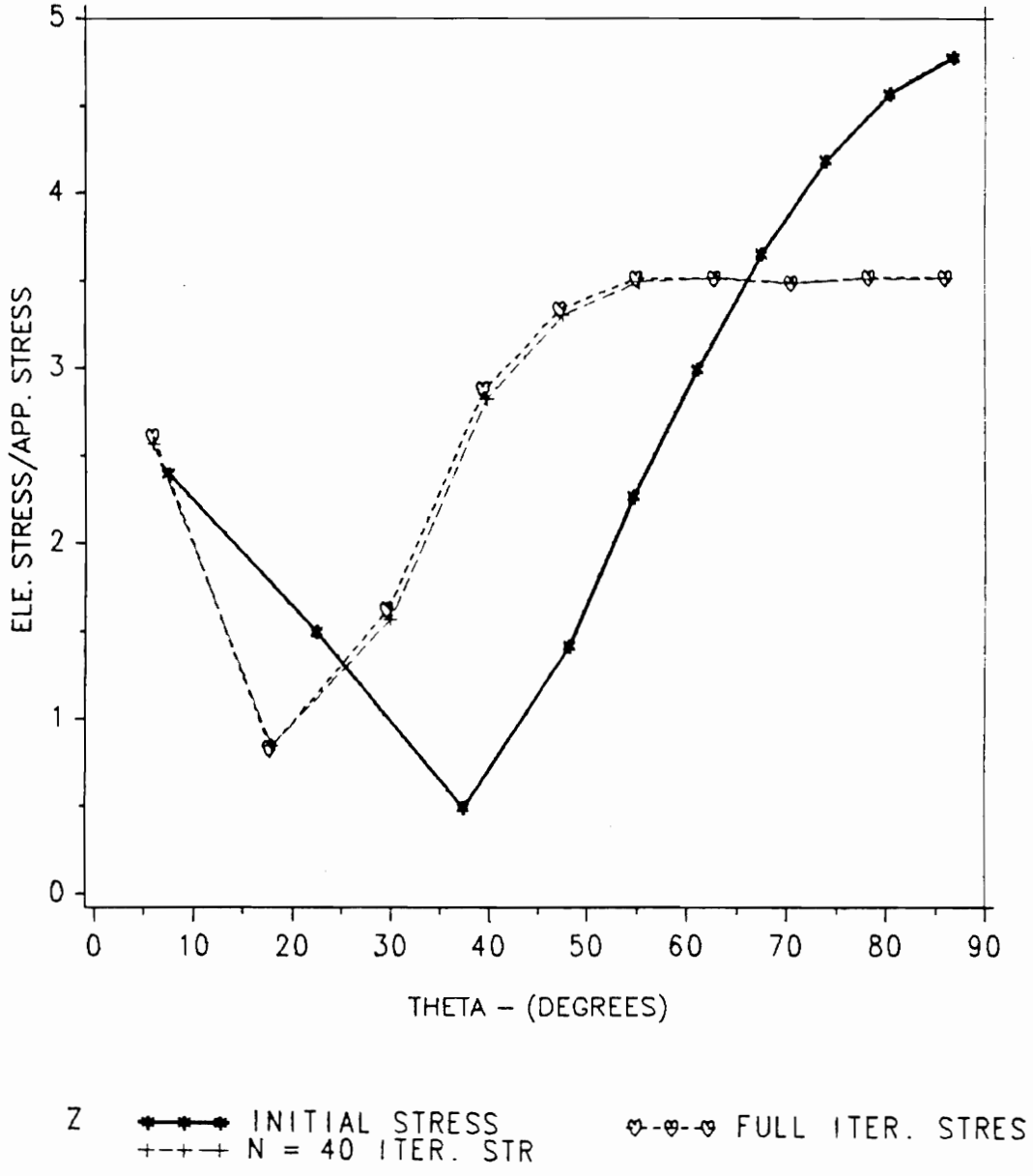

Figure 14. Stress Concentration in Elements Around Hole Boundary (Inexact Forces)

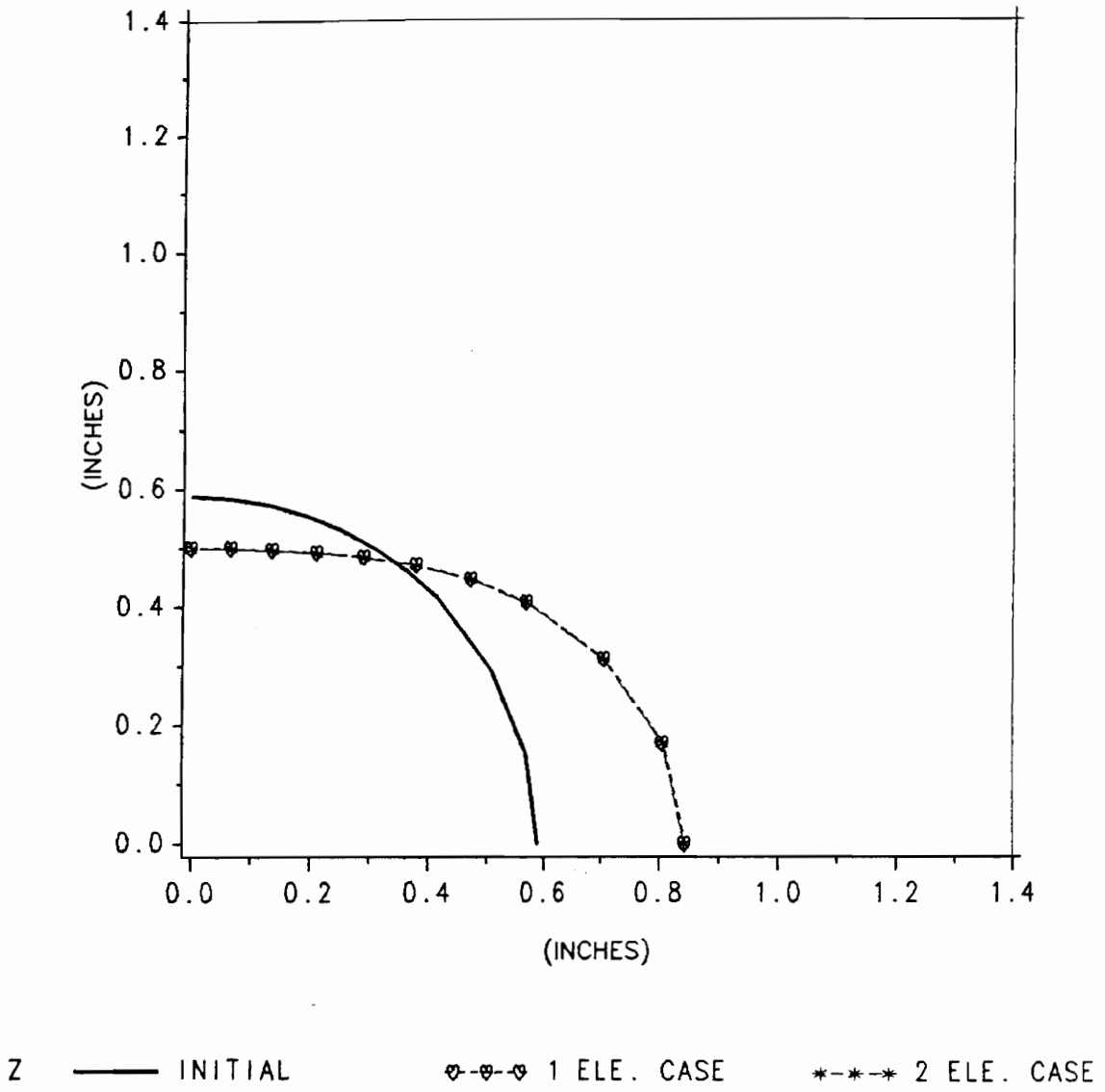

Figure 15. Optimum Hole Shape Comparison for 1 layer and 2 layer cases

Vita

The author was born in Mysore, India on the sixth day of March, 1963. She received her Bachelor of Technology degree in Aeronautical Engineering from the Indian Institute of Technology, Kharagpur, India in May, 1985. In September 1986, she joined the Master of Science program in the Aerospace and Ocean Engineering department at Virginia Tech.